Modeling and optimization of ultrasonic devulcanization using the response surface methodology based on central composite face-centered design

Ivan Mangili [a], Marina Lasagni [a], Keyuan Huang [b], Avraam I. Isayev [b]

[a] Department of Earth and Environmental Sciences, University of Milano-Bicocca, Piazza della Scienza 1, 20126 Milan, Italy

[b] Department of Polymer Engineering, The University of Akron, Akron, OH, USA

Correspondence to Marina Lasagni (e-mail: marina.lasagni@unimib.it), phone n. +390264482834

Ivan Mangili: ivan.mangili@unimib.it

Marina Lasagni: marina.lasagni@unimib.it

Keyuan Huang: kh41@zips.uakron.edu

Avraam I. Isayev: aisayev@uakron.edu

ABSTRACT

The ultrasonic devulcanization of a ground tire rubber in a co-rotating twin-screw extruder was studied and optimized using the response surface methodology based on an experimental design. This approach allowed evaluating the influence on the process of four variables (ultrasonic amplitude, temperature, screw speed and flow rate). The devulcanization process was investigated using several responses, including crosslink density, gel fraction, complex viscosity of the devulcanizates and tensile strength, modulus and elongation at break of the revulcanizates. Regression models and response surfaces were obtained for each response. The results predicted by these models showed good agreement with experimental values. The ultrasonic amplitude was found to be the most effective variable influencing the devulcanization process and mechanical properties. In addition, an optimization was carried out through a desirability function approach, in order to define the combination of process parameters that maximizes the mechanical properties and minimizes the degradation of the tire rubber.

KEYWORDS Ground Tire Rubber, Devulcanization, Central Composite Face-Centered Design, Response Surface Methodology, Ultrasonic Twin-Screw Extruder, Desirability Function.

1 INTRODUCTION

During last decades, the generation of waste rubber products and End of Life Tires (ELTs) is rapidly increasing and it represents a main issue [1]. ELTs are mainly composed of vulcanized rubber. This material could represent a source of rubber for new tires, resulting in a reduction of raw material use. Nevertheless, the presence of three dimensional crosslink network in a vulcanized rubber represents the main obstacle to the recycling of this material, since it is infusible, insoluble and hard to break. Several chemical, thermo-mechanical and physical methods have been studied for reclamation of ELTs [2]. Most of these techniques require the separation of metallic and texture materials and a grinding process leading to a significant reduction of tire rubber dimensions. After a strong reduction in size, the ground tire rubber (GTR) can be reused in new tires as a filler at low percentage, since the introduction of GTR in virgin rubber results in worse mechanical properties. Indeed, the presence of sulfur crosslink network leads to a weak adhesion of GTR particles to the virgin rubber, leading to deterioration of the final properties [3].

The last decade gave birth to a green devulcanization process, employing ultrasound [4]. This process is carried out without involving any chemical, since ultrasound can generate cavitation leading to the rupture of three-dimensional network in the rubber matrix within a time of several seconds. Most of the previous studies investigated this reclaiming process using an ultrasonic single-screw extruder on several types of rubber, in particular, GTR, natural rubber (NR) and various synthetic rubbers. GTR represents an ideal raw material for the ultrasonic devulcanization, since it can be fed directly into the extruder. Recently, the incorporation of an ultrasonic device in a twin-screw extruder makes the process more efficient [5]. The resulting devulcanized tire rubber can be directly compounded with curatives without adding virgin rubber and revulcanized.

Several researches have also investigated a devulcanization process based only on shear stress and high temperature produced in twin-screw extruders at several conditions and varying several screw configurations [6-11]. Most of these devulcanization studies were carried out in order to find the best devulcanization conditions by analyzing the process parameters just considering one-variable-at-a-time (OVAT) [12]. In OVAT approach, the variables that could possibly affect the performances of the process are kept at a fixed level except for one, which is varied until the best conditions are met. Moreover, the devulcanization process on GTR in a twin-screw extruder was investigated using the response surface methodology (RSM) [13-16]. These studies mainly pointed out that temperature, screw speed and flow rate have significant effect on the devulcanization process. Nevertheless, no ultrasonic devulcanization study was carried out by means of RSM.

For process improvement and optimization, it is usually necessary to consider how a number of input variables, such as temperature, feed rate, screw speed, etc. can simultaneously influence experimental responses. Simulations of ultrasonic devulcanization based on physical modeling were performed in [17-19]. The complex nature of ultrasonic devulcanization of GTR, only led to a qualitative agreement between experimental and simulation results, indicating that the process model reported in Isayev *et al.* [17-19] was insufficient for optimization of the process.

Another possibility to develop a process model of ultrasonic devulcanization of GTR is to carry out statistical modeling. The use of statistical experimental design and responses surfaces allows to get a clear picture of how the process variables behave both separately and cooperatively on the experimental responses and how it is possible to control them in order to make the process more effective [12]. Since all the previous physical approaches used to describe, predict and optimize the ultrasonic rubber devulcanization process resulted in really complex systems, this statistical approach offers a useful tool for the optimization of this process within the studied domain for a multi-response situation.

The aim of the present research is to investigate and optimize a multi-response ultrasonic devulcanization process of a GTR in co-rotating twin-screw extruder using the RSM based on central composite face-centered design (CCFD) [20,21]. A similar study using a more classical OVAT approach would require many more experiments, necessary to cover the experimental domain, without estimating the interaction effects among the variables and with the risk to locate the wrong optimum for each response [22,23].

The process variables considered in the present research were those that resulted to be significant in the aforementioned studies with the addition of the ultrasonic amplitude. Several responses, including crosslink density, gel fraction, complex viscosity of devulcanizates, tensile strength, modulus and elongation at break of revulcanizates were analyzed. The variables and interactions with a significant influence on the process were considered in order to define a second-order surface for each response. The multi-response optimization was carried out through a desirability function approach in order to define the combination of factors that maximize the overall level of satisfaction with respect to the responses under study.

2 MATERIALS AND METHODS

2.1 Materials and equipment

The GTR used in the present study was a 40 mesh cryo-ground rubber from truck tires, extensively characterized and treated in our previous studies [24,25]. 95 wt % of the GTR particles were smaller than 0.4 mm with the majority of them being between 0.15 and 0.4 mm. The rubber fraction was 53 % of the total weight and it was made up of 70 % NR and 30 % of synthetic rubber (butadiene rubber and styrene-butadiene rubber).

The devulcanization process was carried out in an ultrasonic co-rotating twin-screw extruder (Prism USALAB 16, Thermo Electron Co., UK) [5]. A water-cooled ultrasonic horn with a 800 W power supply (Branson 2000 bdc, Branson Ultrasonic Co., CT) was operating at 40 kHz, providing a longitudinal ultrasonic wave perpendicular to the flow direction of the material. The cross section of the horn had dimensions of 28x28 mm^2. Energy from a power supply was converted into mechanical energy for the devulcanization. The gap between the horn tip and the screws is 2.5 mm and the volume of ultrasonic treatment zone is 1.54 cm^3. The barrel temperature was monitored by several thermocouples inserted in the barrel. The flow rate was regulated by varying the material feeding rate.

The configuration of the screw elements is shown in Figure 1. Both screws are single-flighted with diameter of 16 mm and L/D ratio of 24. One reverse element was introduced after the ultrasonic zone to guarantee the complete filling of the ultrasonic treatment zone and to increase pressure and residence time of the GTR in this zone. The addition of more reverse elements resulted in extremely high torque.

2.2 Design of experiments

A central composite face-centered experimental design [20,21] was chosen in the present study to model and optimize the ultrasonic devulcanization process and to analyze the effect of each variable, their interactions and second-order terms. It is generated by combining a two-level full factorial design with axial experiments requiring a number of experiments equal to $N = L^k + 2*k + N_c$. L represents the number of levels for the investigation (two in our case), k represents the number of process variables, or factors (four in our case) and N_c is the number of central experiments.

Table 1 shows maximum (coded as +1), minimum (coded as -1) and central (coded as 0) levels for each process variable, including the ultrasonic amplitude (US), screw speed (SS), flow rate (FR) and temperature (T). Each level was chosen by carrying out several trial experiments, considering the type of GTR and the maximum operating level for the equipment in term of maximum torque, screw speed and temperature.

Table 1: Factors and levels of the experimental design.

Factor, Units	Min level	Max level	Central level
Code	-1	+1	0
Ultrasonic amplitude (US), µm	5	12	8.5
Screw speed (SS), rpm	150	250	200
Flow rate (FR), g/min	4	8	6
Temperature (T), ℃	130	210	170

Although just one or two center runs are required for central composite designs [21], four center runs were introduced in the experimental design considering one of the criteria reported by Draper [26]. He suggested to add at least four center runs for a face-centered central composite design. This number is required to achieve adequate pure error degrees of freedom and a reasonably sensitive lack of fit test [26]. The rotatability of central composite designs [20] was sacrificed in the present study by choosing the distance of axial experiments at ±1, due to the experimental complexity to carry out the axial experiments at different levels.

Twenty-eight experiments were carried out to investigate the experimental domain. A fully randomized execution of experiments was carried out in order to minimize the error due to the planning of experiments.

The complex viscosity (η*), crosslink density (CD) and gel fraction (GF) were chosen as experimental responses in order to study the devulcanized GTR (D-GTR). The modulus at 100 % of elongation (M100), tensile strength (TS) and elongation at break (Eb) were chosen as experimental responses in order to study the properties of the revulcanized GTR (R-GTR).

A preliminary regression model, evaluated for each response, was a second-order model containing the four factors, their squares and two-factor interactions. The dependence of each experimental response, y, on the factors was modeled by applying the following equation [20-21]:

$$y = \beta_0 + \sum_{i=1}^{n} \beta_i x_i + \sum_{i=1}^{n} \beta_{ii} x_i^2 + \sum_{i=1}^{n-1} \sum_{j=i+1}^{n} \beta_{ij} x_i x_j + \varepsilon \qquad (1)$$

where β_0 is the constant term, β_i, β_{ii} and β_{ij} are the coefficients, ε is the error, x_i and x_j are the variables (US, SS, FR and T) and n is the number of variables. The coefficients were determined by multiple linear regressions.

The three-factor interaction terms were considered when the experimental observations were not adequately fitted by the second-order model (eq. 1), resulting in a poor model with low coefficients of determination or serious lack of fit. In these cases, the response surface could be more complex than that defined by the second-order approximation model given by equation (1) [27-29].

Model term P-values from the Analysis Of Variance (ANOVA) and the coefficient of determination in prediction (Q^2_{LOO}) were considered to achieve the best subset model [21]. Q^2_{LOO} represents the leave-one-out cross-validated R^2, where the residual sum of square is replaced by the predicted residual sum of square (PRESS) [30-32]. The PRESS is calculated using the following equation:

$$PRESS = \sum_{i=1}^{n}\left(y_i - \hat{y}_{i\setminus i}\right) \qquad (2)$$

where $\hat{y}_{i\setminus i}$ represents the predicted response estimated using a regression model calculated without the i-th observation.

The terms whose P-value was higher than 0.1 were sequentially and systematically eliminated. The terms whose P-value was between 0.1 and 0.05 were kept in the model only if they contributed to an increase of the Q^2_{loo} value. The best reduced model containing only the significant factors, interactions and second-order terms was thus calculated for each experimental response.

2.2.1 Responses for the devulcanized GTR (D-GTR)

The crosslink density, gel fraction and complex viscosity were determined on the D-GTR. These measurements gave information on the degree of devulcanization. Each measurement was repeated at least three times.

Advanced Polymer Analyzer (APA 2000, Alpha Technologies, Akron, OH) was used to determine the dynamic properties of the D-GTR, in particular the complex viscosity. The analyses were carried out at 120 ℃ within a frequency range between 0.15 rad/s a nd 200 rad/s and a strain amplitude of 0.042.

The crosslink density was determined through swelling measurements. 1 g D-GTR (W_1) was extracted for 24 hours in standard Soxhlet using toluene as solvent. After this period of time, the excess of solvent on the sample surface was removed with a paper towel and the swollen sample was weighed. Finally, the sample was dried in vacuum oven for 24 h and weighed again (W_2). The Flory-Rehner equation was used in order to calculate the crosslink density. The χ interaction parameter between rubber (NR) and swelling solvent (toluene) was set equal to 0.39. The density of the NR rubber with incorporation of sulfur was taken to be 0.92 g/cm^3 [33]. The carbon black density was taken to be 1.85 g/cm^3 and the constant C in the Kraus correction model was taken to be 1.17 [34,35]. The content of carbon black was 30 % as determined by thermogravimetric analysis [24].

The gel fraction was also evaluated by the Soxhlet extraction and calculated as:

$$Gel\,fraction\,(\%) = (W_2/W_1) * 100 \quad (3)$$

2.2.2 Responses for the revulcanized GTR (R-GTR)

In order to investigate the mechanical properties, the D-GTR was homogenized and compounded with curatives using a two – roll mill (Reliable Rubber & Plastic Machinery Co., North Bergen, NJ) for 10 and 30 passes, respectively. The chemicals used for the compounding recipe were courteously donated by Akrochem Corporation (Akron, OH, USA) and were added as follows: 1 part per hundred of rubber (phr) powder N-cyclohexyl-2-benzothiazole sulfenamide, 1 phr rubbermakers sulfur, 1.25 phr RGT-M zinc oxide and 0.25 phr rubber grade stearic acid, based on 100 phr of D-GTR.

The curing behavior of the D-GTR samples at 160 °C was studied using the APA 2000 by performing a time sweep, at a frequency of 10 rad/s and a strain amplitude of 0.042. The resulting curves were used to evaluate the optimum curing time for the tensile test. R-GTR sheets of 15x15 cm^2 with thickness varying from 2.2 to 3.5 mm were prepared using a compression-molding press (Carver, Wabash, IN) at the optimum curing time (t_{95}). The dumbbell shape specimens for tensile test (type C in the ASTM D 412 standard method) were cut out from those sheets. Mechanical properties were measured at room temperature using tensile testing machine (Instron tensile tester, Model 5567, Instron), following the ASTM D 412 standard method, at an elongation rate of 500 mm/min. Tensile strength, modulus at 100 % of elongation and elongation at break were evaluated on at least five R-GTR samples.

2.3 Optimization

Desirability functions were used to define the optimum condition for the treatment [36]. The desirability function approach (d_i) assigns numbers ranging between 0 and 1 for each response $y_i(x)$. The individual desirability functions are then combined in order to find the most desirable condition with respect to all the responses. Two different desirability functions were employed to maximize the overall level of satisfaction with respect to all the responses.

2.3.1 Derringer and Suich desirability functions

Two different types of desirability functions [37] were considered according to the response characteristics. Both of them transform the response for each combination of experimental conditions into a value lying between 0 and 1, where 1 is the best condition and 0 represents the worst one. The larger-the-best (LTB) and the smaller-the-best (STB) desirability functions were respectively calculated as:

$$d_i(x) = \begin{cases} 0\,, & \hat{y}_i(x) \le y_i^{min} \\ \left(\frac{\hat{y}_i(x) - y_i^{min}}{y_i^{max} - y_i^{min}}\right)^r, & y_i^{min} < \hat{y}_i(x) < y_i^{max} \\ 1\,, & \hat{y}_i(x) \ge y_i^{max} \end{cases} \qquad LTB \qquad (4)$$

$$d_i(x) = \begin{cases} 1\,, & \hat{y}_i(x) \le y_i^{min} \\ \left(\frac{\hat{y}_i(x) - y_i^{max}}{y_i^{min} - y_i^{max}}\right)^r, & y_i^{min} < \hat{y}_i(x) < y_i^{max} \\ 0\,, & \hat{y}_i(x) \ge y_i^{max} \end{cases} \qquad STB \qquad (5)$$

where y_i^{max} and y_i^{min} represent the maximum and minimum tolerance limits, ($\hat{y}_i$(x)) are the estimated responses and r, having positive values, represent the weights. The LTB, reported in equation 4, is used when the value of the estimated response is expected to be larger than a lower tolerance limit. The STB, reported in equation 5, is used when the value of the estimated response is expected to be smaller than an upper tolerance limit.

In a multi-response situation, the overall desirability function (*D*) is maximized and represented by a geometric mean obtained by combining the individual desirability functions (d_i) defined as:

$$\max_{x\in\Omega} D = \left(\prod_{i=1}^{n} d_i^{w_i}\right)^{\frac{1}{\sum_{i=1}^{n} w_i}} \tag{6}$$

where d_i is the individual desirability function of the i-th response, x represents the combination of experimental conditions within the experimental domain Ω and w_i are the weights assigned to each response. A high w_i implies that the desirability value is close to 0, unless the response gets very close to its target value. Higher w_i values assign more importance to the d_i. The objective of this approach is to find the experimental conditions, maximizing the D value within the experimental domain.

2.3.2 Kim and Lin desirability functions

In this approach [38], the individual desirability function of i-th response, d_i, has an exponential form and it is defined as:

$$d'(z) = \begin{cases} \frac{\exp(t') - exp(t'|z|)}{exp(t') - 1}, & t = 0 \\ 1 - |z|, & t \neq 0 \end{cases} \tag{7}$$

where $t' = t + (1 - R^2)(t^{max} - t)$ and t^{max} is a sufficient large value of t (constant, $-\infty<t<\infty$) such that d′(z) with t^{max} is a concave curve assuming virtually no effect in the optimization process. Realistic values of t lies between -10 and 10. For $t < 0$ the function is convex, for $t = 0$ the function is linear and for $t > 0$ the function is concave. R^2 is the coefficient of determination and z is a standardized parameter representing the distance of the estimated response from its target in units of the maximum allowable deviation. This parameter depends on the response type and is defined as:

$$z_i(x) = \begin{cases} \frac{\hat{y}_i(x) - y_i^{min}}{y_i^{max} - y_i^{min}}, & (for\ STB) \\ \frac{y_i^{max} - \hat{y}_i(x)}{y_i^{max} - y_i^{min}}, & (for\ LTB) \end{cases} \qquad with\ y_i^{min} \leq \hat{y}_i(x) \leq y_i^{max} \tag{8}$$

where y_i^{max} and y_i^{min} represent the maximum and minimum values of the estimated response ($\hat{y}_i$(x)), respectively. Eq. (8) between 0 and 1.

In the present study, in order to consider the predictive ability of each response model, R^2 was substituted by the coefficient of determination in prediction (Q^2_{LOO}). t^{max} was fixed equal to 10. The values of *t* for each model were chosen considering the importance of the response.

In this approach, the overall minimal level of satisfaction is reached following the formulation:

$$\max_{x\in\Omega}(\min\,[d_1\,\{(\hat{y}_1(x)\}, d_2\{(\hat{y}_2(x)\}, \ldots d_n\{(\hat{y}_n(x)\}]) \tag{9}$$

where x represents the combination of experimental conditions within the experimental domain Ω.

In the present study, only LTB and STB response types were considered for both approaches. The minimum and maximum values for each responses (y_i^{max} and y_i^{min}) were set at the extreme values of each estimated response.

The linear regression models, ANOVA, response surfaces and desirability functions were calculated by Modde 6.0 (Umetrics, Umea, Sweden), and MATLAB R2013 (The MathWorks Inc., Natick, USA).

3 RESULTS AND DISCUSSION

3.1 Regression models

The results of the experiments are summarized in Table 2. As a response for the model, the value of η* was uniquely taken at the frequency of 200 rad/s, since the analysis was more stable at this frequency.

For each experimental response, a reduced subset model was obtained considering the only terms that resulted significant. Table 3 shows regression coefficients for each experimental response related to the scaled and centered variables.

In order to achieve the best subset model, some terms were included even if they did not result significant to preserve the principal of hierarchy. A model is considered hierarchical if the presence of significant higher-interactions or higher-order terms requires the inclusion of the lower-order terms within the higher-order ones.

All the obtained reduced regression models were statistically significant at 95% level, without showing any lack of fit at the same probability [12,21]. The residual distributions, as shown in Figure 2, did not reveal evident anomalies. The normal distribution for the residuals was confirmed by the Shapiro-Wilk normality test at 99 % confidence level [39].

Q^2_{LOO} was used to select the best subset model for each response. Therefore, this statistic resulted in the highest prediction power for each model (Table 4). Moreover, each model showed relatively high R^2 and R^2 adjusted (R^2 adj), offering an acceptable explanation of the total variance.

Table 2 Results of the central composite design.

Experiment	US (µm)	SS (rpm)	FR (g/min)	T (℃)	η* (kPa.s)	CD (mmol/cm^3)	GF (wt %)	M100 (MPa)	TS (MPa)	Eb (elongation %)
Experiments based on a full factorial design at two levels										
E1	5	150	4	130	3.26	0.043	83.0	3.22	4.52	132
E2	12	150	4	130	1.90	0.028	75.5	2.71	5.37	169
E3	5	250	4	130	3.53	0.040	85.0	3.43	4.21	117
E4	12	250	4	130	1.34	0.020	74.0	2.53	5.88	179
E5	5	150	8	130	4.03	0.043	84.2	3.49	4.43	127
E6	12	150	8	130	2.23	0.032	77.0	3.01	4.71	136
E7	5	250	8	130	3.79	0.031	83.2	3.50	3.86	112
E8	12	250	8	130	1.63	0.024	76.5	2.56	6.52	196
E9	5	150	4	210	3.09	0.027	81.3	3.19	4.02	124
E10	12	150	4	210	1.70	0.028	76.1	2.48	4.70	161
E11	5	250	4	210	1.75	0.028	79.1	3.12	6.10	159
E12	12	250	4	210	1.00	0.018	74.4	2.86	6.13	179
E13	5	150	8	210	3.35	0.035	83.6	3.19	3.52	112
E14	12	150	8	210	2.07	0.027	77.7	2.62	4.89	162
E15	5	250	8	210	2.01	0.023	77.8	2.89	6.06	170
E16	12	250	8	210	1.28	0.020	74.8	2.60	6.22	189
Axial experiments (distance ± 1 from the center)										
E17	5	200	6	170	3.77	0.037	84.1	3.38	4.11	116
E18	12	200	6	170	2.16	0.026	77.4	3.05	5.65	160
E19	8.5	150	6	170	3.01	0.033	80.7	3.10	4.27	133
E20	8.5	250	6	170	1.81	0.023	77.4	3.03	6.02	163
E21	8.5	200	4	170	2.09	0.029	77.7	2.83	5.92	174
E22	8.5	200	8	170	2.54	0.030	79.3	2.90	4.96	152
E23	8.5	200	6	130	2.62	0.038	80.5	3.20	4.97	150
E24	8.5	200	6	210	1.58	0.027	77.8	2.87	6.35	178
Central experiments										
C1	8.5	200	6	170	2.37	0.033	79.1	2.97	5.42	160
C2	8.5	200	6	170	2.59	0.028	78.6	2.84	5.09	158
C3	8.5	200	6	170	2.48	0.027	78.6	3.13	5.39	142
C4	8.5	200	6	170	2.51	0.027	77.9	3.19	5.00	140

Table 3 Regression coefficients and standard error (SE) for each experimental response related to the scaled and centered variables.

Experimental response	η*	SE	CD	SE	GF	SE	M100	SE	TS	SE	Eb	SE
Constant	2.45	0.05	0.0295	0.0004	79.0	0.2	3.05	0.03	5.3	0.1	153	3
US	-0.74	0.04	-0.0047	0.0005	-3.2	0.2	-0.28	0.02	0.51	0.09	20	2
SS	-0.36	0.04	-0.0038	0.0005	-0.9	0.2	-0.03	0.02	0.59	0.09	12	2
FR	0.18	0.04	0.0002	0.0005	0.4	0.2	0.02	0.02	_	_	-2	2
T	-0.36	0.04	-0.0037	0.0005	-0.9	0.2	-0.10	0.02	0.20	0.09	6	2
US*US	0.40	0.09	_	_	1.1	0.4	0.13	0.05	-0.3	0.1	-14	5
SS*SS	_†	_	_	_	_	_	_	_	_	_	_	_
FR*FR	_	_	_	_	-1.1	0.4	-0.22	0.05	_	_	_	_
T*T	-0.47	0.09	_	_	_	_	_	_	_	_	12	5
US*SS	-0.02E-05	0.04	-0.0004	0.0005	0.2E-01	0.2	-0.01	0.02	0.08	0.09	3	2
US*FR	_	_	0.0009	0.0005	0.3	0.2	_	_	_	_	_	_
US*T	0.21	0.04	0.0021	0.0005	0.8	0.2	0.06	0.02	-0.20	0.09	-4	2
SS*FR	_	_	-0.0012	0.0005	-0.4	0.2	-0.07	0.02	_	_	5	2
SS*T	-0.19	0.04	_	_	-0.7	0.2	0.03	0.02	0.37	0.09	6	2
FR*T	_	_	0.0003	0.0005	_	_	-0.06	0.02	_	_	_	_
US*SS*FR	_	_	0.0016	0.0005	0.4	0.2	_	_	_	_	_	_
US*SS*T	0.15	0.04	_	_	0.4	0.2	0.10	0.02	-0.32	0.09	-9	2
US*FR*T	_	_	-0.0012	0.0005	_	_	_	_	_	_	_	_
SS*FR*T	_	_	_	_	_	_	_	_	_	_	_	_

† The character '_' represents the coefficient removed from the reduced model.

Table 4 Coefficients of determinations of reduced models

Response	R^2	R^2 adj	Q^2_{LOO}	$y_i^{min\dagger}$	$y_i^{max\dagger}$	Optimal
η*	0.98	0.96	0.94	0.80	4.16	Min
CD	0.93	0.89	0.86	0.018	0.044	Min
GF	0.98	0.95	0.88	73.8	85.3	Min
M100	0.94	0.90	0.88	2.52	3.67	Max
TS	0.87	0.81	0.74	3.69	6.46	Max
EB	0.91	0.85	0.72	194	102	Max

† The value of y_i^{min} and y_i^{max} were computed for each response

3.1.2 D-GTR

η* was determined as a function of the angular frequency and followed the power law behavior. Therefore, the experimental data were fitted according to the following equation:

$$\eta^* = K\omega^{n-1} \tag{10}$$

where *ω* represents the frequency and *K* and n are empirical constants (n < 1).

The constant *K* in Eq. 10, representing a measure of flow resistance, could have been used as an additional experimental response for the model. This parameter allowed us to consider the behavior of the rubber in the entire region of the studied frequencies. Figure 3 shows the dependence of η* on the frequency ω and the power law fit for three samples chosen as representative ones.

Nevertheless, this additional response (K) showed an analogous behavior as η* at 200 rad/s with the same significant terms for the fitted reduced model. For this reason, it was decided to uniquely consider η* during the optimization process.

The analysis of the η*, GF and CD were performed directly on the material after the devulcanization, since these values give information on the rupture of the crosslink network. The η*, as function of angular frequency, is a measure of the resistance to flow. In particular η* decreases with a decrease of molecular weight, crosslink density and gel fraction. The GF represents the insoluble fraction after removing the sol fraction. It decreases with the increase of network breakage and with the increase of polymeric soluble fraction. Similarly, the CD represents the effective number of chains per unit of volume and it decreases with the increase of devulcanization.

From the reduced models (Table 3), it can be seen that all process variables have influence on the devulcanization process. The ultrasonic amplitude showed the highest effect, acting with a negative trend on D-GTR properties. Indeed, as already observed in [4], the ultrasonic devulcanization increases with the ultrasonic amplitude. The effects of screw speed and temperature were found to be less important despite the fact that these process variables acted in the same direction as the ultrasonic amplitude. Indeed these two process variables are responsible for thermal and mechanical degradation and decrosslinking [8,9]. The effect of flow rate was observed to be less important and acting in opposite direction, since the flow rate increase decreases the residence time of the material within the extruder, decreasing the devulcanization treatment time.

In order to investigate in more detail the relative effect of degradation of the main chain and of the crosslink network, the normalized gel fraction versus the normalized crosslink density (Figure 4) was studied. Since it is difficult to determine the type of bond rupture during the ultrasonic treatment of GTR, the dependence of experimental normalized gel fraction versus normalized crosslink density was analyzed and compared to the Horikx function, that was derived from the statistical theory dealing with the gel fraction–crosslink density relationship [34,40-45]. In our case, it was possible to calculate only the function for the main chain brakeage, but not the one for the selective crosslink breakage, since the value of M_n is not available for the GTR that represents a waste and vulcanized material. Thus, in Figure 4, the line indicates the Horikx function based on the main chain breakage only. Experimental data are indicated by symbols. It is seen that experimental results lie above the Horikx function [44]. Therefore, it can be concluded that the ultrasonic treatment preferentially cleaved the crosslink network with some breakage of the main chain. However, it is impossible from this plot to define types of crosslink breakage (mono-sulfidic, di-sulfidic and poly-sulfidic). In addition, it was difficult to experimentally measure the amount of different type crosslink breakage on D-GTR. In that regard, a previous study [45] (conducted on a model SBR rubber) indicated that the ultrasonic devulcanization causes a significant decrease of poly-sulfidic and mono-sulfidic crosslinks indicating that ultrasonic devulcanization takes place indeed.

3.1.3 R-GTR

The analysis of M100, TS and Eb were performed on the material R-GTR after compounding and revulcanization. Generally, the compound recipe and crosslink network type are the main parameters influencing all these mechanical properties [46]. However, in our case, the filler content and recipe of the R-GTR were kept constant. Therefore, the mechanical properties were strictly correlated to the devulcanization effect induced by the ultrasonic treatment.

M100 is a measure of the tensile properties at 100 % of elongation. TS and Eb represent the final mechanical properties. They define the failure point of the vulcanizates.

As seen from Table 3, M100 follows a reduced model that is similar to the one observed for all the responses evaluated on the D-GTR. The increase of the ultrasonic amplitude, screw speed and temperature and the decrease of the flow rate led to lower values of M100. Several researches have already observed that the modulus increases with the crosslink density and gel fraction of the material. Furthermore, the crosslink density and gel fraction of revulcanizates are highly correlated with the correspondent devulcanizates, as long as the curing recipe is kept constant [5,47]. Therefore, also in this case higher values of gel fraction and crosslink density of D-GTR led to higher values of R-GTR. Although M100 of R-GTR resulted to be correlated with the crosslink density and gel fraction of the D-GTR, it is clear that TS and Eb behaved differently. Indeed, the main significant process variables had completely opposite influence on these two properties. These final mechanical properties were strongly influenced by the degree of devulcanization. More breakage of the three-dimensional network can generate more active sites that can be cured during the revulcanization process, increasing the compatibility among the D-GTR particles.

In order to better understand the trend of the response surfaces, 3D plot are shown in Figure 5. In these surfaces each response was plotted as function of US and T, fixing the values of FR at center level (0) and SS at the highest one (+ 1).

In Figure 5 it is clear that the mechanical properties are strongly dependent on the structure properties. Namely, the CD, GF and η* showed similar behaviors, since their decrease was observed with an increase of T and US. On the other hand, the mechanical properties did not show a unique behavior. The M100 showed significant decrease at high T and US, while the opposite was observed for TS and Eb. As already observed in the previous study [5] this different behavior of the mechanical properties of the R-GTR can be explained by considering their correlation with the structure of the D-GTR. The reduction of CD and GF is generally associated to an increase of the sol fraction. This soluble polymeric fraction, along with the gel of lower crosslink density, provides enough active sites that can be re-cured, increasing the compatibility among various D-GTR particles, resulting in better final properties. On the other hand, the M100 behaves in opposite manner since this property shows higher values at higher values of CD and GF.

3.2 Validation

A validation was carried out in order to test the reduced models predictive power within the studied domain. In addition, some experiments were carried out to evaluate the applicability of the model outside the studied domain.

The conditions used for validation experiments are reported in Table 5. These experiments were fixed by selecting combinations of independent variables within the experimental domain. Moreover, the predictive power of the models was tested outside the experimental region, removing the most influential process variable. Therefore, two experiments (v1 and v2) were carried out without applying any ultrasonic treatment.

The results of these validation experiments are shown in Figure 6. In particular, the experimental results of the validation experiments (v1-v7) are represented by symbols and are compared to the range of values predicted by each model, here presented as bars. It can be seen that the validation experiments carried out within the experimental domain (v3-v7) were in good agreement with the range of predicted values. Moreover, some models showed an acceptable predictive capacity outside the experimental range (v1 and v2).

Table 5 Validation experiment conditions.

Experiment	Ultrasonic Amplitude (µm)	Screw Speed (rpm)	Flow rate (g/min)	Temperature (℃)
		Experiments out of the experimental domain		
v1	0	250	8	130
v2	0	200	8	170
		Experiments within the experimental domain		
v3	8.5	250	6	170
v4	8.5	200	6	170
v5	12	250	6	130
v6	12	200	6	170
v7	12	150	8	130

3.3 Optimization

In the previous sections, our attention was focused on modeling each response as a function of the input process variables. Two different behaviors were generally observed, as seen in Figure 5. Moreover, in Figure 7 it can be observed that the optimal condition as a function of US and T is different for each response.

Although, for practical applications, the process variables could be varied in order to achieve the optimal conditions for a desired property, in the present study a multiple response optimization approach was attempted. In particular, this optimization was carried out considering a possible application of the D-GTR in new tires. Therefore, it was decided to assign more importance to the M100 and TS. The weights and parameters used for the two different desirability function approaches are shown in Table 6. The results of the optimization are listed in Table 7.

Although the two desirability function approaches gave different overall degree of satisfaction, the two approaches gave comparable results in term of optimal process conditions. In order to maximize the value of M100 and TS, it is necessary to keep a relatively low value of US, sufficient to reduce the network density and to increase the number of active sites so D-GTR can be revulcanized, without introducing an excessive degradation.

Table 6 Parameters for desirability functions

Response	Type of desirability function	$y_i^{min\dagger}$	$y_i^{max\dagger}$	w‡	t§
η*	STB	0.80	4.16	1	-1
CD	STB	0.018	0.044	1	-1
GF	STB	73.8	85.3	1	-1
M100	LTB	2.52	3.67	3	-3
TS	LTB	3.69	6.46	3	-3
EB	LTB	194	102	1	-1

† The value of y_i^{min} and y_i^{max} were computed for each response, using the reduced subset models reported in the Results and Discussion section.
‡ Weights for the Derringer and Suich approach
§ Value of t parameter for the Kim and Lin approach

Table 7 Desirability functions optimization results

Parameter	Derringer and Suich	Kim and Lin
Optimal Conditions (US, SS, FR, T)	(7.2, 250, 5.5, 210)	(5, 250, 5.6, 202)
Predicted responses (η*, CD, GF, M100, TS, Eb)	(1.22, 0.023, 77.4, 3.03, 6.39, 183)	(2.16, 0.027, 80.2, 3.27, 5.87, 155)
Desirability function value optimal conditions d (η*, CD, GF, M100, TS, Eb)	(0.87, 0.79, 0.69, 0.09, 0.93, 0.88) †	(0.55, 0.73, 0.48, 0.48, 0.82, 0.80) †
Overall degree of satisfaction	0.71	0.48

† Each d (η*, CD, GF, M100, TS, Eb) was already weighed considering the parameters in Table 6.

4 CONCLUSIONS

The aim of the present study was to investigate a green and continuous ultrasonic devulcanization process that could be carried out in a short time adjusting the process variables in order to optimize specific required conditions. Ultrasonic-assisted devulcanization in a twin-screw extruder was studied and modeled using a face-centered central composite design and desirability functions. Several responses on the D-GTR and on R-GTR were chosen as responses and reduced regression models were obtained by regression analysis. The properties of the D-GTR and R-GTR were influenced by all the process variables as well as interaction effects between them. However, the US was found to be the most influencing process variable for the described screw configuration. Different behaviors were observed for the various responses. For this reason, an optimization was performed in order to maximize the TS and M100, considered the most important parameters for reuse of D-GTR. A relatively low value of US was required to reduce the network density without introducing an excessive degradation of the tire rubber.

This study has an important outcome since the approach presented here can be applied to the devulcanization of any type of GTR in order to reach the optimal desirable properties for different applications.

ACKNOWLEDGEMENTS

The authors are grateful to the financial support provided by the National Science Foundation (NSF) under Grant CMMI-1131342 and to Akrochem Corporation for providing compounding ingredients. The authors also thank Dr. Paola Caracino for the support given to our research.

REFERENCES

1. B. Adhikari, D. De, S. Maiti, Reclamation and recycling of waste rubber, Prog. Polym. Sci. 25 (2000) 909-948.

2. V. Rajan, W.K. Dierkes, R. Joseph, J.W.M. Noordermeer, Science and technology of rubber reclamation with special attention to NR-based waste latex products, Prog. Polym. Sci. 31 (2006) 811-834.

3. A.K. Naskar, S.K. De, A.K. Bhowmick, P.K. Pramanik, R. Mukhopadhyay, Characterization of ground rubber tire and its effect on natural rubber compound, Rubber Chem. Technol.73 (2000) 902-911.

4. A.I. Isayev, Recycling of Rubbers, in: J.E. Mark, B. Erman, M. Roland (Eds.), The Science and Technology of Rubber, fourth ed., Elsevier Academic Press, Boston: 2014., pp. 697-764.

5. A.I. Isayev, T. Liang, T.M. Lewis, Effect of particle size on ultrasonic devulcanization in twin-screw extruder, Rubber Chem. Technol. 87 (2014) 86-102.

6. K. Formela, M. Cysewska, J. Haponiuk, A. Stasiek, The influence of feed rate and shear forces on the devulcanization process of ground tire rubber (GTR), Polimery 58 (2013)906-912.

7. K. Formela, M. Cysewska, J. Haponiuk, The influence of screw configuration and screw speed of co-rotating twin screw extruder on the properties of products obtained by thermomechanical reclaiming of ground tire rubber, Polimery 59 (2014) 170-177.

8. J. Shi, K. Jiang, D. Ren, H. Zou, Y. Wang, X. Lv, L. Zhang, Structure and performance of reclaimed rubber obtained by different methods, J. Appl. Polym. Sci. 129 (2013) 999-1007.

9. G. Tao, Q. He, Y. Xia, G. Jia, H. Yang, W. Ma, The effect of devulcanization level on mechanical properties of reclaimed rubber by thermal-mechanical shearing devulcanization, J. Appl. Polym. Sci. 129 (2013) 2598-2605.

10. B. Maridass, Cure modeling and mechanical properties of counter rotating twin screw extruder devulcanized ground rubber tire-natural rubber blends, J. Polym. Res. 16 (2009) 133-141.

11. H. Si, T. Chen, Zhang Y, Effects of High Shear Stress on the Devulcanization of Ground Tire Rubber in a Twin-Screw Extruder, J. Appl. Polym. Sci. 128 (2013) 2307-2318.

12. G.P.E. Box, W.G. Hunter, J.S. Hunter, Statistics for Experimenters, second ed., Wiley, Hoboken, New Jersey: 1978.

13. B. Maridass, B.R. Gupta, Effect of extruder parameters on mechanical properties of revulcanized ground rubber tire powder. Polimery 52 (2007) 456-460.

14. B. Maridass, B.R. Gupta, Process optimization of devulcanization of waste rubber powder from syringe stoppers by twin screw extruder using response surface methodology, Polym. Compos 29 (2008) 1350-1357.

15. H. Yazdani, I. Ghasemi, M. Karrabi, H. Azizi, G.R. Bakhshandeh, Continuous devulcanization of waste tires by using a co-rotating twin screw extruder: Effects of screw configuration, temperature profile, and devulcanization agent concentration, J. Vinyl. Addit. Technol. 19 (2013) 65-72.

16. B. Maridass, B.R. Gupta, Performance optimization of a counter rotating twin screw extruder for recycling natural rubber vulcanizates using response surface methodology, Polym. Test. 23 (2004) 377-385.

17. A.I. Isayev, S.P. Yushanov, J. Chen, Ultrasonic devulcanization of rubber vulcanizates. I. Process model. J. Appl. Polym. Sci. 59 (1996) 803-813.

18. A.I. Isayev, S.P. Yushanov, J. Chen, Ultrasonic devulcanization of rubber vulcanizates. II. Simulation and experiment, J. Appl. Polym. Sci. 59 (1996) 815-824.

19. S.P. Yushanov, A.I. Isayev, S.H. Kim, Ultrasonic Devulcanization of SBR Rubber: Experimentation and Modeling Based on Cavitation and Percolation Theories, Rubber. Chem. Technol. 71 (1998) 168-190.

20. I. Khuri, J.A. Cornell, Response Surfaces: Designs and Analyses, second ed., Marcel and Dekker Inc., New York, 1996.

21. R.H. Myers, D.C. Montgomery, Response surface methodology: process and product optimization using designed experiments, second ed. Wiley, New York, 2002.

22. P.J. Brandvik, Statistical simulation as an effective tool to evaluate and illustrate the advantage of experimental designs and response surface methods, Intell. Lab. Syst.42 (1998) 51–61.

23. Leardi R. Experimental design in chemistry: A tutorial, Anal. Chim. Acta 652 (2009) 161–172.

24. I. Mangili, E. Collina, M. Anzano, D. Pitea, M. Lasagni, Characterization and supercritical CO2 devulcanization of cryo-ground tire rubber: Influence of devulcanization process on reclaimed material, Polym. Degrad. Stabil.102 (2014) 15-24.

25. I. Mangili, M. Oliveri, M. Anzano, E. Collina, D. Pitea, M. Lasagni, Full factorial experimental design to study the devulcanization of ground tire rubber in supercritical carbon dioxide, J. Supercrit. Fluids 92 (2014) 249-256.

26. N.R Draper, Center points in second-order response surface designs, Technometrics 24 (1982) 127-133.

27. J.A. Dec, N.M. Thornblom Autonomous Aerobraking: Thermal Analysis and Response Surface Development. Adv. Astronaut Sci.142 (2012) 483-498.

28. L.A. Dillon, V.N. Stone, L.A. Croasdell, P.R. Fielden, N.J. Goddard, C.L. Thomas, Optimisation of secondary electrospray ionisation (SESI) for the trace determination of gas-phase volatile organic compounds, Analyst 135 (2010) 306-314.

29. E. Cagigal, L. González, R.M. Alonso, R.M. Jiménez, Experimental design methodologies to optimise the spectrofluorimetric determination of Losartan and Valsartan in human urine, Talanta 54 (2001) 1121-1133.

30. L. Eriksson, E. Johansson, N. Kettaneh-Wold, C. Wikström and S. Wold, Design of Experiments Principles and Applications, third ed., Umetrics Academy, Umea, 2008.

31. I.E. Frank, R. Todeschini, The data analysis handbook, Elsevier, Amsterdam, 1994.

32. I. Batmaz, S. Tunali, Second-Order Experimental Designs for Simulation Metamodeling, Simulation:78 (2002) 699-715.

33. J.L. Valentín, J. Carretero-González, I. Mora-Barrantes, W. Chassé, K. Saalwa□chter, Uncertainties in the determination of crosslink density by equilibrium swelling experiments in Natural Rubber. Macromolecules 41 (2008) 4717-4729.

34. E. Bilgili, H. Arastoopour, B. Bernstein, Pulverization of rubber granulates using the solid state shear extrusion process. Part II. Powder characterization. Powder Technol. 115 (2001) 277-289.

35. G. Kraus, Swelling of filler-reinforced vulcanizates, J. Appl. Polym. Sci.7 (1963) 861-871.

36. N.R. Costa, J. Lourenço, Pereira. Desirability function approach: A review and performance evaluation in adverse conditions, Chemometr. Intell. Lab. 107 (2011) 234-244.

37. G. Derringer, R. Suich, Simultaneous Optimization of Several Response Variables. J. Qual. Technol.12 (1980) 214-219.

38. K.J. Kim, D. Lin, Simultaneous optimization of multiple responses by maximining exponential desirability functions, J. Roy. Stat. Soc. C-App.49 (2000) 311-325.

39. S.S. Shapiro, M.B. Wilk, An analysis of variance test for normality (complete samples). Biometrika 52 (1965) 591-611.

40. X. Sun, A.I. Isayev, Ultrasound devulcanization: comparison of synthetic isoprene and natural rubbers, J. Mater. Sci.42 (2007) 7520-7529.

41. S. Ghose, A.I. Isayev, Ultrasonic devulcanization of carbon black filled polyurethane rubber, J. Elastom. Plast.36 (2004) 213-239.

42. VV. Yashin, A.I. Isayev, A model for rubber degradation under ultrasonic treatment: part II. Rupture of rubber network and comparison with experiments, Rubber Chem. Technol.73 (2000) 325-338.

43. A.I. Isayev, S. P. Yushanov, S.H. Kim, V.L. Levin, Ultrasonic devulcanization of waste rubbers: experimentation and modeling, Rheol. Acta 35 (1996) 616-630.

44. M.M. Horikx, Chain scissions in a polymer network, J. Polym. Sci. 19 (1956) 445-454

45. V. Yu Levin, S. H. Kim, A. I. Isayev, Effect of Crosslink Type on the Ultrasound Devulcanization of SBR Vulcanizates. Rubber Chem. Techol. 70 (1997) 641-649.

46. A.Y. Coran, Vulcanization, in: J.E. Mark, B. Erman, M. (Eds.), The Science and Technology of Rubber, fourth ed. Elsevier Academic Press,Boston: 2014., pp. 337-381.

47. W. Feng, A.I Isayev, In-situ ultrasonic compatibilization of unvulcanized and dynamically vulcanized PP/EPDM blends, Polym. Eng. Sci. 46 (2006) 8-16.

Captions

Figure 1 Schematic of the screw configuration.

Figure 2 Normal probability plot of residuals for η*(a), CD (b), GF (c), TS (d), M100 (e) and Eb (d).

Figure 3 Power law fitting examples on samples E1 (a), E12 (b) and C4 (c) corresponding to Table 2.

Figure 4 Normalized gel fraction as function of normalized crosslink density compared to the Horikx function.

Figure 5 Responses surfaces of η* (a), CD (b), GF (c), M100 (d), TS (e), and Eb (f) as function of T and US at highest value of SS (250 rpm) and middle value of FR (6 g/min).

Figure 6 Results of validation experiments (V1-V7 in Table 5) represented by symbols compared to the range of predicted values at 95 % confidence level (shown as bars).

Figure 7 Contour plots of η* (a), CD (b), GF (c), M100 (d), TS (e), and Eb (f) as function of T and US at highest value of SS (250 rpm) and middle value of FR (6 g/min). Black color represents the optimal condition for each response.

Figure 1
Click here to download high resolution image

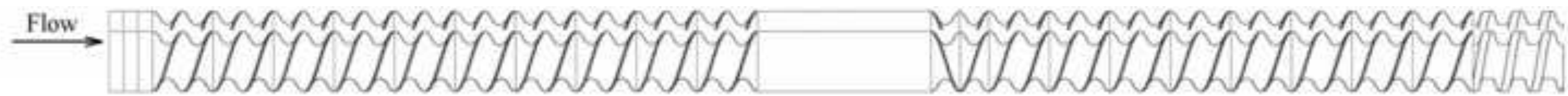

Figure 2

Click here to download high resolution image

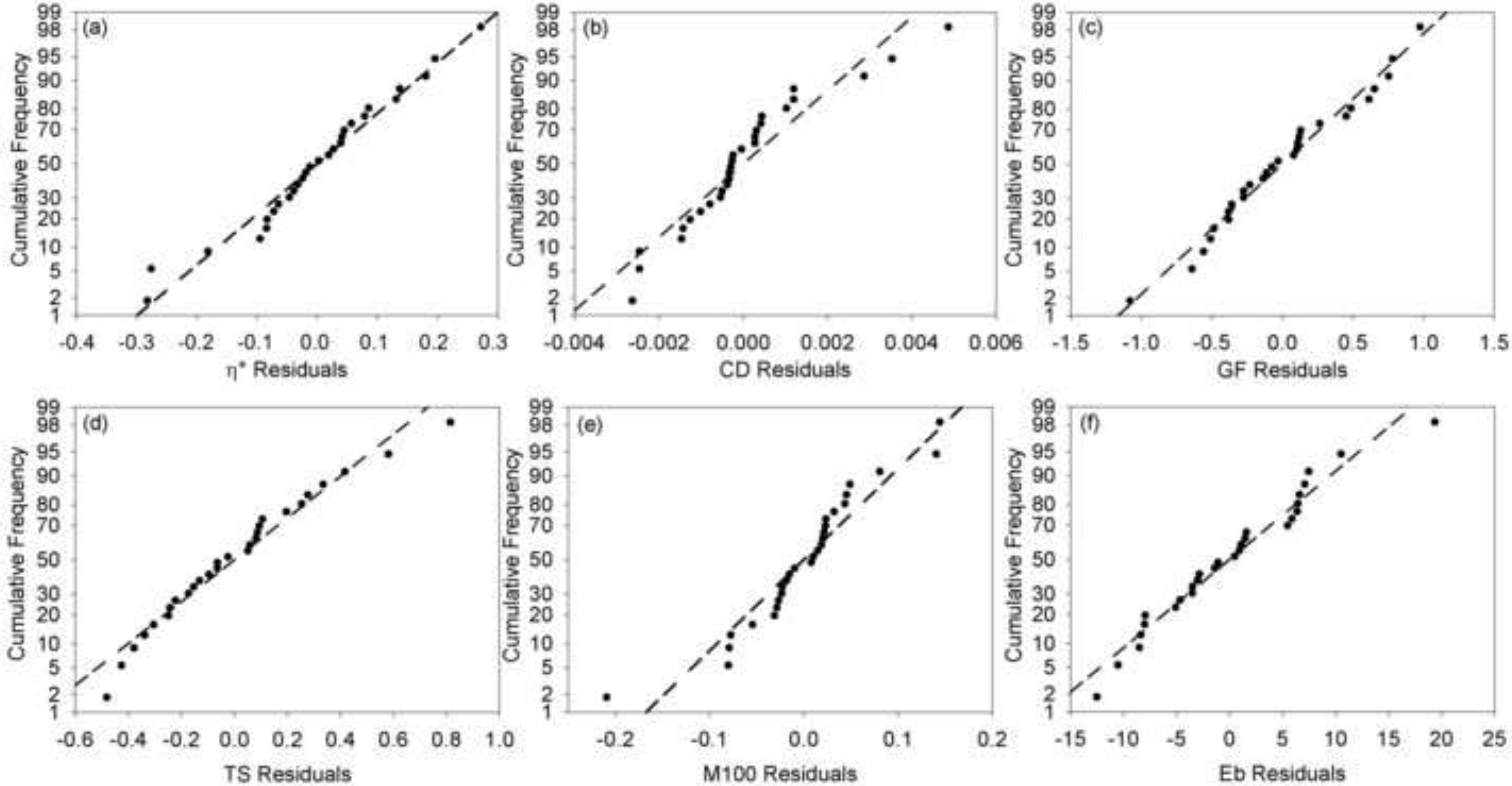

Figure 3
Click here to download high resolution image

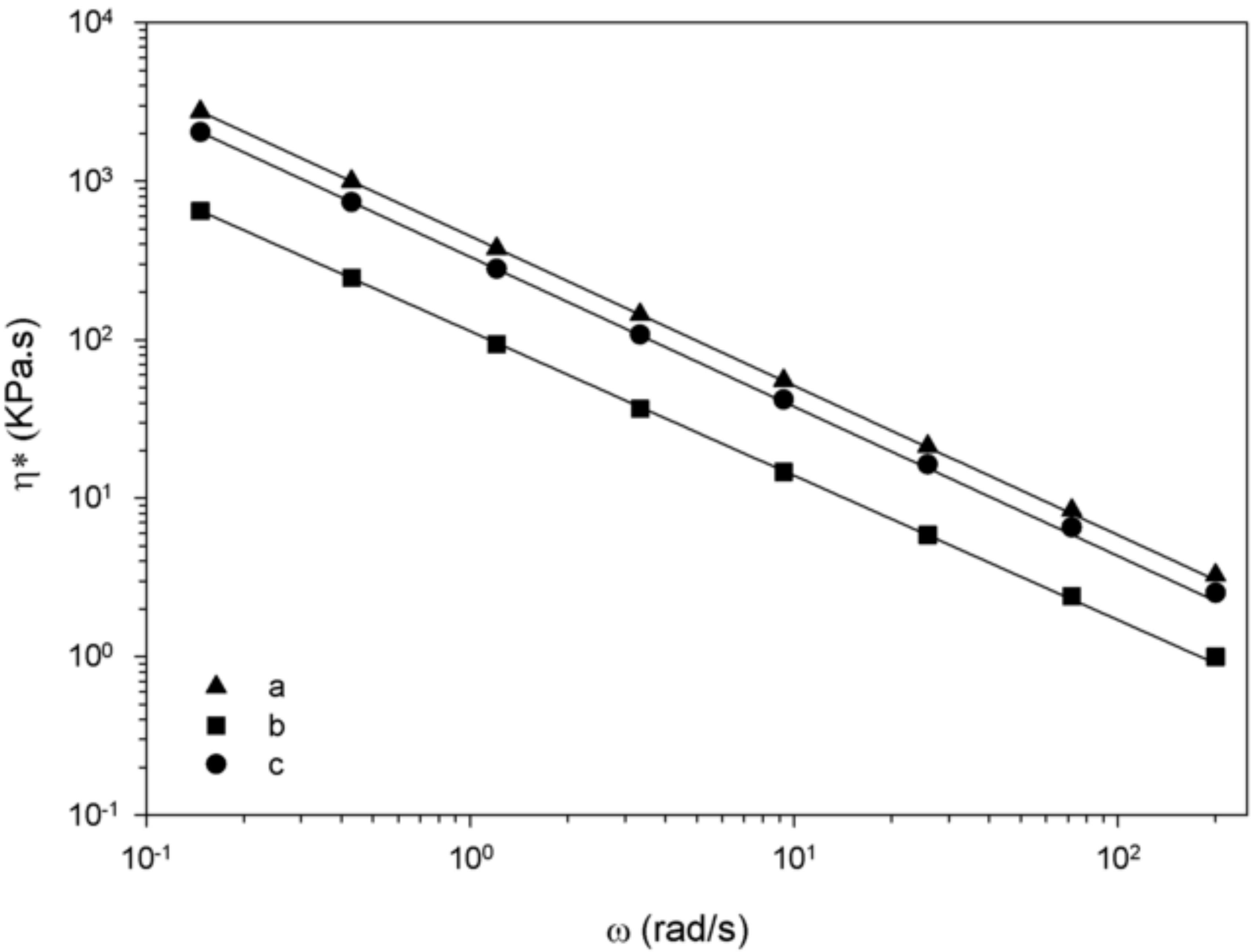

Figure 4
Click here to download high resolution image

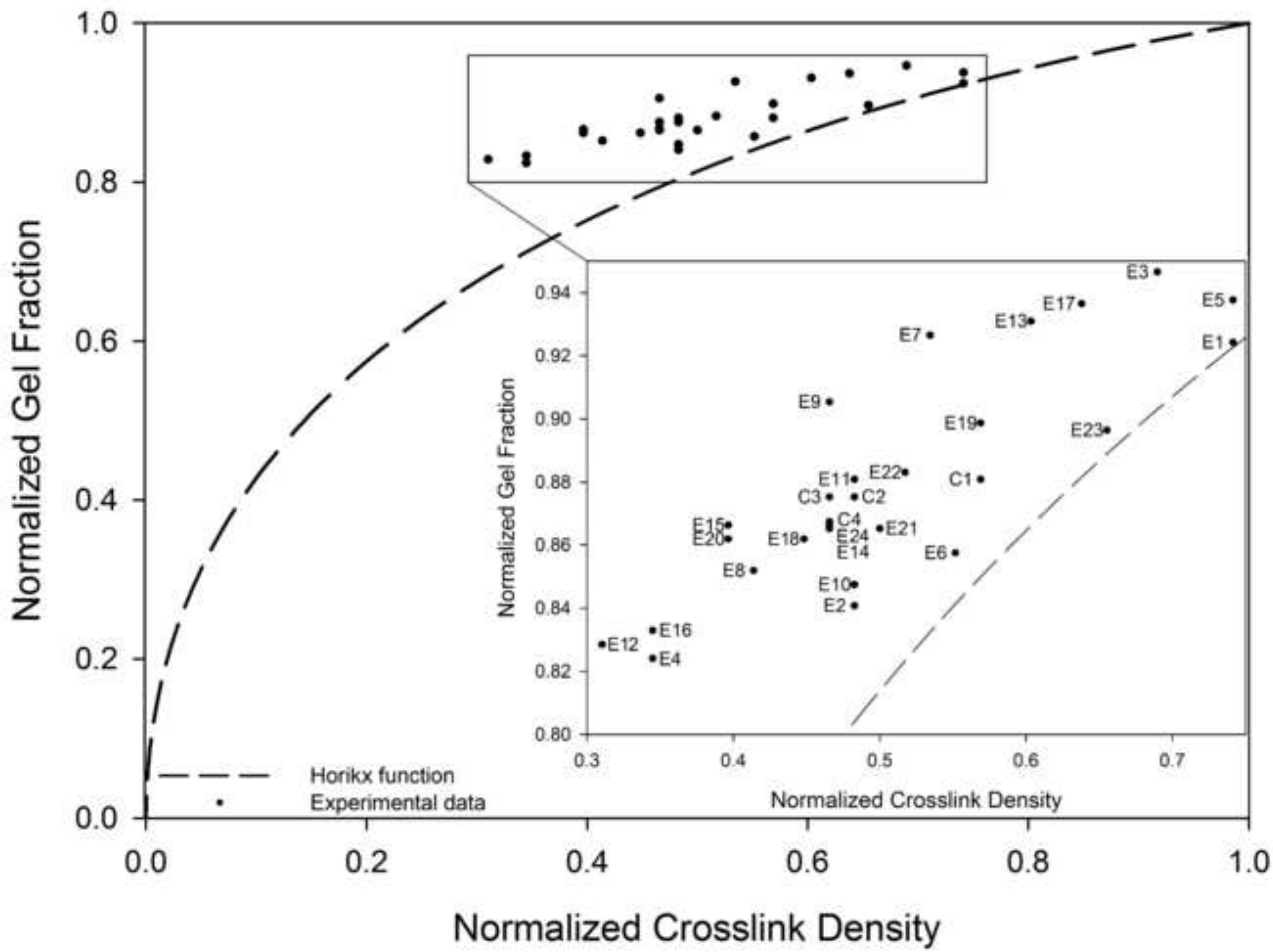

Figure 5
Click here to download high resolution image

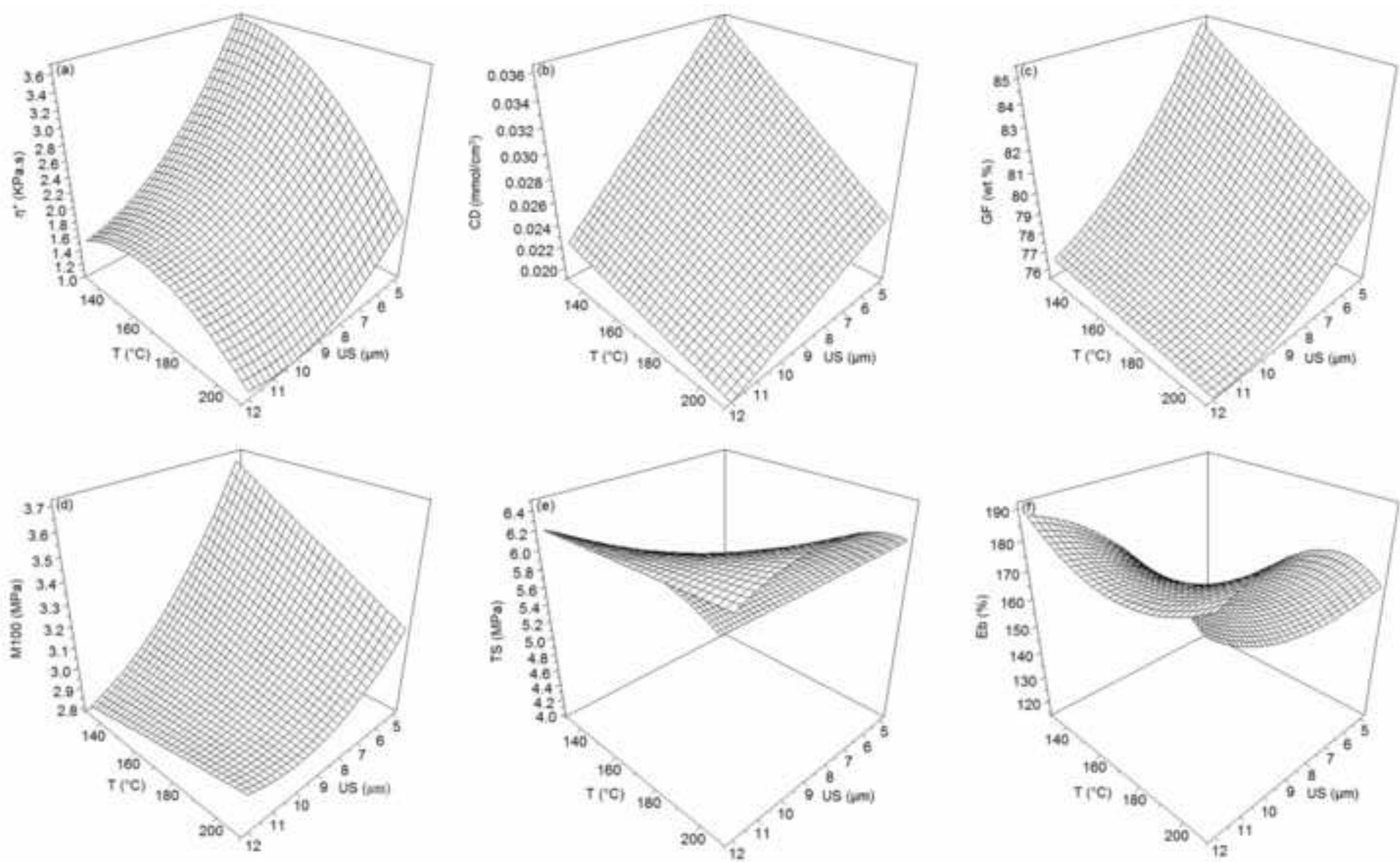

Figure 6
Click here to download high resolution image

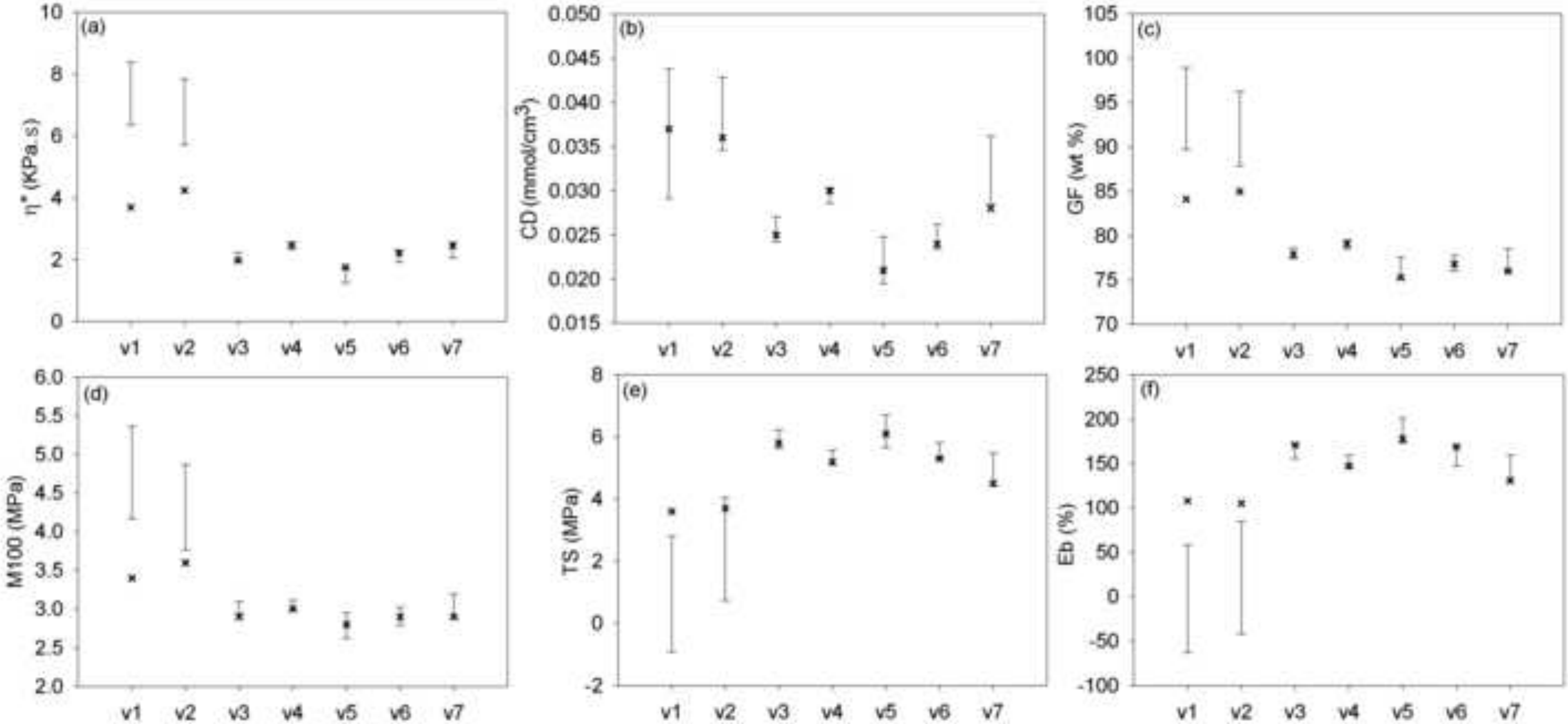

Figure 7

Click here to download high resolution image

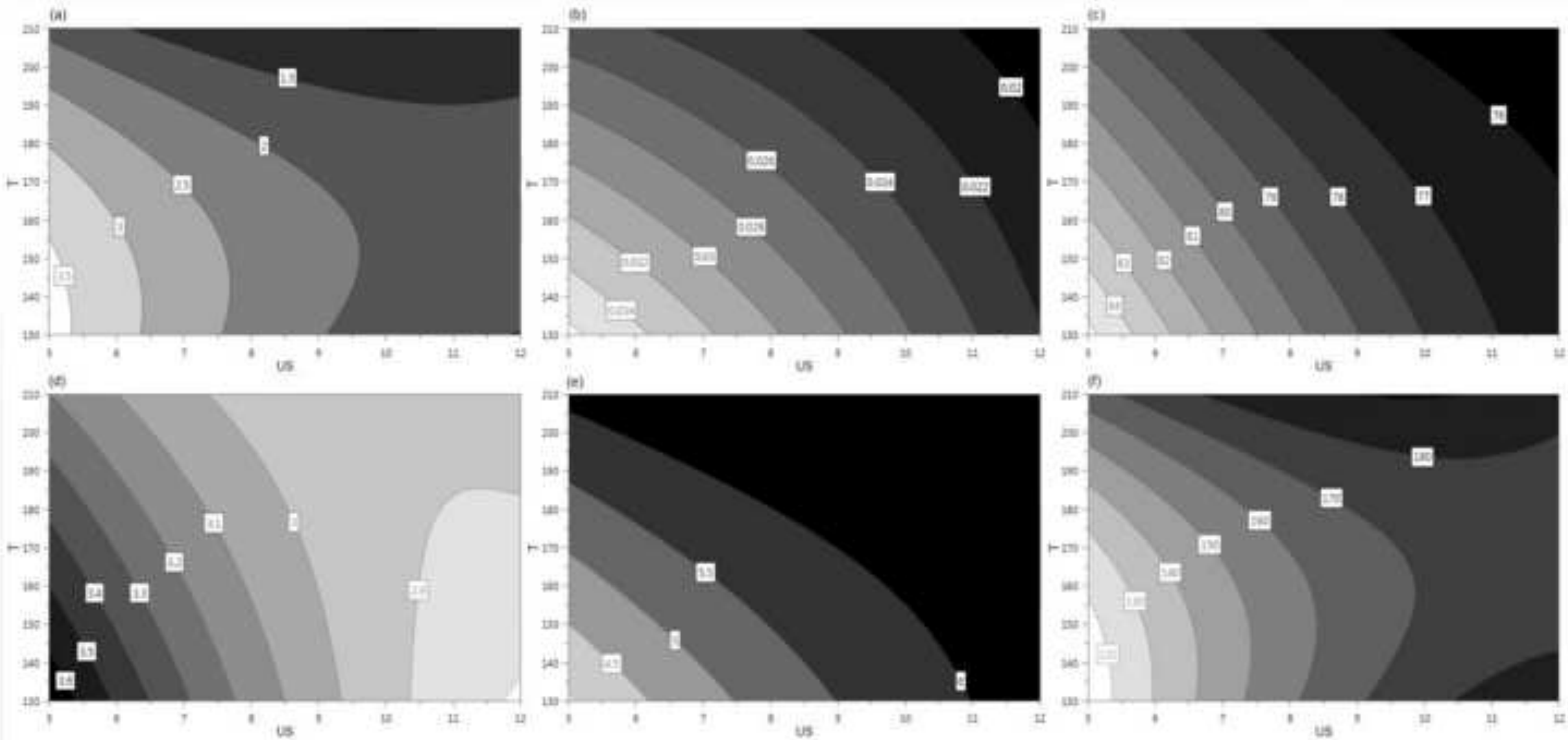

Modeling and optimization of ultrasonic devulcanization using the response surface methodology based on central composite face-centered design

Ivan Mangili [a], Marina Lasagni [a], Keyuan Huang [b], Avraam I. Isayev [b]

[a] Department of Earth and Environmental Sciences, University of Milano-Bicocca, Piazza della Scienza 1, 20126 Milan, Italy

[b] Department of Polymer Engineering, The University of Akron, Akron, OH, USA

Correspondence to Marina Lasagni (e-mail: marina.lasagni@unimib.it), phone n. +390264482834

Ivan Mangili: ivan.mangili@unimib.it

Marina Lasagni: marina.lasagni@unimib.it

Keyuan Huang: kh41@zips.uakron.edu

Avraam I. Isayev: aisayev@uakron.edu

ABSTRACT

The ultrasonic devulcanization of a ground tire rubber in a co-rotating twin-screw extruder was studied and optimized using the response surface methodology based on an experimental design. This approach allowed evaluating the influence on the process of four variables (ultrasonic amplitude, temperature, screw speed and flow rate). The devulcanization process was investigated using several responses, including crosslink density, gel fraction, complex viscosity of the devulcanizates and tensile strength, modulus and elongation at break of the revulcanizates. Regression models and response surfaces were obtained for each response. The results predicted by these models showed good agreement with experimental values. The ultrasonic amplitude was found to be the most effective variable influencing the devulcanization process and mechanical properties. In addition, an optimization was carried out through a desirability function approach, in order to define the combination of process parameters that maximizes the mechanical properties and minimizes the degradation of the tire rubber.

KEYWORDS Ground Tire Rubber, Devulcanization, Central Composite Face-Centered Design, Response Surface Methodology, Ultrasonic Twin-Screw Extruder, Desirability Function.

1 INTRODUCTION

During last decades, the generation of waste rubber products and End of Life Tires (ELTs) is rapidly increasing and it represents a main issue [1]. ELTs are mainly composed of vulcanized rubber. This material could represent a source of rubber for new tires, resulting in a reduction of raw material use. Nevertheless, the presence of three dimensional crosslink network in a vulcanized rubber represents the main obstacle to the recycling of this material, since it is infusible, insoluble and hard to break. Several chemical, thermo-mechanical and physical methods have been studied for reclamation of ELTs [2]. Most of these techniques require the separation of metallic and texture materials and a grinding process leading to a significant reduction of tire rubber dimensions. After a strong reduction in size, the ground tire rubber (GTR) can be reused in new tires as a filler at low percentage, since the introduction of GTR in virgin rubber results in worse mechanical properties. Indeed, the presence of sulfur crosslink network leads to a weak adhesion of GTR particles to the virgin rubber, leading to deterioration of the final properties [3].

The last decade gave birth to a green devulcanization process, employing ultrasound [4]. This process is carried out without involving any chemical, since ultrasound can generate cavitation leading to the rupture of three-dimensional network in the rubber matrix within a time of several seconds. Most of the previous studies investigated this reclaiming process using an ultrasonic single-screw extruder on several types of rubber, in particular, GTR, natural rubber (NR) and various synthetic rubbers. GTR represents an ideal raw material for the ultrasonic devulcanization, since it can be fed directly into the extruder. Recently, the incorporation of an ultrasonic device in a twin-screw extruder makes the process more efficient [5]. The resulting devulcanized tire rubber can be directly compounded with curatives without adding virgin rubber and revulcanized.

Several researches have also investigated a devulcanization process based only on shear stress and high temperature produced in twin-screw extruders at several conditions and varying several screw configurations [6-11]. Most of these devulcanization studies were carried out in order to find the best devulcanization conditions by analyzing the process parameters just considering one-variable-at-a-time (OVAT) [12]. In OVAT approach, the variables that could possibly affect the performances of the process are kept at a fixed level except for one, which is varied until the best conditions are met. Moreover, the devulcanization process on GTR in a twin-screw extruder was investigated using the response surface methodology (RSM) [13-16]. These studies mainly pointed out that temperature, screw speed and flow rate have significant effect on the devulcanization process. Nevertheless, no ultrasonic devulcanization study was carried out by means of RSM.

For process improvement and optimization, it is usually necessary to consider how a number of input variables, such as temperature, feed rate, screw speed, etc. can simultaneously influence experimental responses. Simulations of ultrasonic devulcanization based on physical modeling were performed in [17-19]. The complex nature of ultrasonic devulcanization of GTR, only led to a qualitative agreement between experimental and simulation results, indicating that the process model reported in Isayev *et al.* [17-19] was insufficient for optimization of the process.

Another possibility to develop a process model of ultrasonic devulcanization of GTR is to carry out statistical modeling. The use of statistical experimental design and responses surfaces allows to get a clear picture of how the process variables behave both separately and cooperatively on the experimental responses and how it is possible to control them in order to make the process more effective [12]. Since all the previous physical approaches used to describe, predict and optimize the ultrasonic rubber devulcanization process resulted in really complex systems, this statistical approach offers a useful tool for the optimization of this process within the studied domain for a multi-response situation.

The aim of the present research is to investigate and optimize a multi-response ultrasonic devulcanization process of a GTR in co-rotating twin-screw extruder using the RSM based on central composite face-centered design (CCFD) [20,21]. A similar study using a more classical OVAT approach would require many more experiments, necessary to cover the experimental domain, without estimating the interaction effects among the variables and with the risk to locate the wrong optimum for each response [22,23].

The process variables considered in the present research were those that resulted to be significant in the aforementioned studies with the addition of the ultrasonic amplitude. Several responses, including crosslink density, gel fraction, complex viscosity of devulcanizates, tensile strength, modulus and elongation at break of revulcanizates were analyzed. The variables and interactions with a significant influence on the process were considered in order to define a second-order surface for each response.

The multi-response optimization was carried out through a desirability function approach in order to define the combination of factors that maximize the overall level of satisfaction with respect to the responses under study.

2 MATERIALS AND METHODS

2.1 Materials and equipment

The GTR used in the present study was a 40 mesh cryo-ground rubber from truck tires, extensively characterized and treated in our previous studies [24,25]. 95 wt % of the GTR particles were smaller than 0.4 mm with the majority of them being between 0.15 and 0.4 mm. The rubber fraction was 53 % of the total weight and it was made up of 70 % NR and 30 % of synthetic rubber (butadiene rubber and styrene-butadiene rubber).

The devulcanization process was carried out in an ultrasonic co-rotating twin-screw extruder (Prism USALAB 16, Thermo Electron Co., UK) [5]. A water-cooled ultrasonic horn with a 800 W power supply (Branson 2000 bdc, Branson Ultrasonic Co., CT) was operating at 40 kHz, providing a longitudinal ultrasonic wave perpendicular to the flow direction of the material. The cross section of the horn had dimensions of 28x28 mm^2. Energy from a power supply was converted into mechanical energy for the devulcanization. The gap between the horn tip and the screws is 2.5 mm and the volume of ultrasonic treatment zone is 1.54 cm^3. The barrel temperature was monitored by several thermocouples inserted in the barrel. The flow rate was regulated by varying the material feeding rate.

The configuration of the screw elements is shown in Figure 1. Both screws are single-flighted with diameter of 16 mm and L/D ratio of 24. One reverse element was introduced after the ultrasonic zone to guarantee the complete filling of the ultrasonic treatment zone and to increase pressure and residence time of the GTR in this zone. The addition of more reverse elements resulted in extremely high torque.

2.2 Design of experiments

A central composite face-centered experimental design [20,21] was chosen in the present study to model and optimize the ultrasonic devulcanization process and to analyze the effect of each variable, their interactions and second-order terms. It is generated by combining a two-level full factorial design with axial experiments requiring a number of experiments equal to $N = L^k + 2*k + N_c$. L represents the number of levels for the investigation (two in our case), k represents the number of process variables, or factors (four in our case) and N_c is the number of central experiments.

Table 1 shows maximum (coded as +1), minimum (coded as -1) and central (coded as 0) levels for each process variable, including the ultrasonic amplitude (US), screw speed (SS), flow rate (FR) and temperature (T). Each level was chosen by carrying out several trial experiments, considering the type of GTR and the maximum operating level for the equipment in term of maximum torque, screw speed and temperature.

Table 1: Factors and levels of the experimental design.

Factor, Units	Min level	Max level	Central level
Code	-1	+1	0
Ultrasonic amplitude (US), µm	5	12	8.5
Screw speed (SS), rpm	150	250	200
Flow rate (FR), g/min	4	8	6
Temperature (T), ℃	130	210	170

Although just one or two center runs are required for central composite designs [21], four center runs were introduced in the experimental design considering one of the criteria reported by Draper [26]. He suggested to add at least four center runs for a face-centered central composite design. This number is required to achieve adequate pure error degrees of freedom and a reasonably sensitive lack of fit test [26]. The rotatability of central composite designs [20] was sacrificed in the present study by choosing the distance of axial experiments at ±1, due to the experimental complexity to carry out the axial experiments at different levels.

Twenty-eight experiments were carried out to investigate the experimental domain. A fully randomized execution of experiments was carried out in order to minimize the error due to the planning of experiments.

The complex viscosity (η*), crosslink density (CD) and gel fraction (GF) were chosen as experimental responses in order to study the devulcanized GTR (D-GTR). The modulus at 100 % of elongation (M100), tensile strength (TS) and elongation at break (Eb) were chosen as experimental responses in order to study the properties of the revulcanized GTR (R-GTR).

A preliminary regression model, evaluated for each response, was a second-order model containing the four factors, their squares and two-factor interactions. The dependence of each experimental response, y, on the factors was modeled by applying the following equation [20-21]:

$$y = \beta_0 + \sum_{i=1}^{n} \beta_i x_i + \sum_{i=1}^{n} \beta_{ii} x_i^2 + \sum_{i=1}^{n-1} \sum_{j=i+1}^{n} \beta_{ij} x_i x_j + \varepsilon \qquad (1)$$

where β_0 is the constant term, β_i, β_{ii} and β_{ij} are the coefficients, ε is the error, x_i and x_j are the variables (US, SS, FR and T) and n is the number of variables. The coefficients were determined by multiple linear regressions.

The three-factor interaction terms were considered when the experimental observations were not adequately fitted by the second-order model (eq. 1), resulting in a poor model with low coefficients of determination or serious lack of fit. In these cases, the response surface could be more complex than that defined by the second-order approximation model given by equation (1) [27-29].

Model term P-values from the Analysis Of Variance (ANOVA) and the coefficient of determination in prediction (Q^2_{Loo}) were considered to achieve the best subset model [21]. Q^2_{Loo} represents the leave-one-out cross-validated R^2, where the residual sum of square is replaced by the predicted residual sum of square (PRESS) [30-32]. The PRESS is calculated using the following equation:

$$PRESS = \sum_{i=1}^{n} \left(y_i - \hat{y}_{i \setminus i} \right) \quad (2)$$

where $\hat{y}_{i \setminus i}$ represents the predicted response estimated using a regression model calculated without the i-th observation.

The terms whose P-value was higher than 0.1 were sequentially and systematically eliminated. The terms whose P-value was between 0.1 and 0.05 were kept in the model only if they contributed to an increase of the Q^2_{loo} value. The best reduced model containing only the significant factors, interactions and second-order terms was thus calculated for each experimental response.

2.2.1 Responses for the devulcanized GTR (D-GTR)

The crosslink density, gel fraction and complex viscosity were determined on the D-GTR. These measurements gave information on the degree of devulcanization. Each measurement was repeated at least three times.

Advanced Polymer Analyzer (APA 2000, Alpha Technologies, Akron, OH) was used to determine the dynamic properties of the D-GTR, in particular the complex viscosity. The analyses were carried out at 120 ℃ within a frequency range between 0.15 rad/s a nd 200 rad/s and a strain amplitude of 0.042.

The crosslink density was determined through swelling measurements. 1 g D-GTR (W_1) was extracted for 24 hours in standard Soxhlet using toluene as solvent. After this period of time, the excess of solvent on the sample surface was removed with a paper towel and the swollen sample was weighed. Finally, the sample was dried in vacuum oven for 24 h and weighed again (W_2). The Flory-Rehner equation was used in order to calculate the crosslink density. The χ interaction parameter between rubber (NR) and swelling solvent (toluene) was set equal to 0.39. The density of the NR rubber with incorporation of sulfur was taken to be 0.92 g/cm^3 [33]. The carbon black density was taken to be 1.85 g/cm^3 and the constant C in the Kraus correction model was taken to be 1.17 [34,35]. The content of carbon black was 30 % as determined by thermogravimetric analysis [24].

The gel fraction was also evaluated by the Soxhlet extraction and calculated as:

$$Gel\ fraction\ (\%) = (W_2/W_1) * 100 \quad (3)$$

2.2.2 Responses for the revulcanized GTR (R-GTR)

In order to investigate the mechanical properties, the D-GTR was homogenized and compounded with curatives using a two – roll mill (Reliable Rubber & Plastic Machinery Co., North Bergen, NJ) for 10 and 30 passes, respectively. The chemicals used for the compounding recipe were courteously donated by Akrochem Corporation (Akron, OH, USA) and were added as follows: 1 part per hundred of rubber (phr) powder N-cyclohexyl-2-benzothiazole sulfenamide, 1 phr rubbermakers sulfur, 1.25 phr RGT-M zinc oxide and 0.25 phr rubber grade stearic acid, based on 100 phr of D-GTR.

The curing behavior of the D-GTR samples at 160 ℃ was studied using the APA 2000 by performing a time sweep, at a frequency of 10 rad/s and a strain amplitude of 0.042. The resulting curves were used to evaluate the optimum curing time for the tensile test. R-GTR sheets of 15x15 cm^2 with thickness varying from 2.2 to 3.5 mm were prepared using a compression-molding press (Carver, Wabash, IN) at the optimum curing time (t_{95}). The dumbbell shape specimens for tensile test (type C in the ASTM D 412 standard method) were cut out from those sheets. Mechanical properties were measured at room temperature using tensile testing machine (Instron tensile tester, Model 5567, Instron), following the ASTM D 412 standard method, at an elongation rate of 500 mm/min. Tensile strength, modulus at 100 % of elongation and elongation at break were evaluated on at least five R-GTR samples.

2.3 Optimization

Desirability functions were used to define the optimum condition for the treatment [36]. The desirability function approach (d_i) assigns numbers ranging between 0 and 1 for each response $y_i(x)$. The individual desirability functions are then combined in order to find the most desirable condition with respect to all the responses. Two different desirability functions were employed to maximize the overall level of satisfaction with respect to all the responses.

2.3.1 Derringer and Suich desirability functions

Two different types of desirability functions [37] were considered according to the response characteristics. Both of them transform the response for each combination of experimental conditions into a value lying between 0 and 1, where 1 is the best condition and 0 represents the worst one. The larger-the-best (LTB) and the smaller-the-best (STB) desirability functions were respectively calculated as:

$$d_i(x) = \begin{cases} 0\,, & \hat{y}_i(x) \leq y_i^{min} \\ \left(\frac{\hat{y}_i(x) - y_i^{min}}{y_i^{max} - y_i^{min}}\right)^r, & y_i^{min} < \hat{y}_i(x) < y_i^{max} \\ 1\,, & \hat{y}_i(x) \geq y_i^{max} \end{cases} \qquad LTB \qquad (4)$$

$$d_i(x) = \begin{cases} 1\,, & \hat{y}_i(x) \leq y_i^{min} \\ \left(\frac{\hat{y}_i(x) - y_i^{max}}{y_i^{min} - y_i^{max}}\right)^r, & y_i^{min} < \hat{y}_i(x) < y_i^{max} \\ 0\,, & \hat{y}_i(x) \geq y_i^{max} \end{cases} \qquad STB \qquad (5)$$

where y_i^{max} and y_i^{min} represent the maximum and minimum tolerance limits, ($\hat{y}_i$(x)) are the estimated responses and r, having positive values, represent the weights. The LTB, reported in equation 4, is used when the value of the estimated response is expected to be larger than a lower tolerance limit. The STB, reported in equation 5, is used when the value of the estimated response is expected to be smaller than an upper tolerance limit.

In a multi-response situation, the overall desirability function (*D*) is maximized and represented by a geometric mean obtained by combining the individual desirability functions (d_i) defined as:

$$\max_{x \in \Omega} D = \left(\prod_{i=1}^{n} d_i^{\,w_i}\right)^{\frac{1}{\sum_{i=1}^{n} w_i}} \quad (6)$$

where d_i is the individual desirability function of the i-th response, x represents the combination of experimental conditions within the experimental domain Ω and w_i are the weights assigned to each response. A high w_i implies that the desirability value is close to 0, unless the response gets very close to its target value. Higher w_i values assign more importance to the d_i. The objective of this approach is to find the experimental conditions, maximizing the D value within the experimental domain.

2.3.2 Kim and Lin desirability functions

In this approach [38], the individual desirability function of i-th response, d_i, has an exponential form and it is defined as:

$$d'(z) = \begin{cases} \frac{\exp(t') - exp(t'|z|)}{exp(t') - 1}, & t = 0 \\ 1 - |z|, & t \neq 0 \end{cases} \quad (7)$$

where $t' = t + (1 - R^2)(t^{max} - t)$ and t^{max} is a sufficient large value of t (constant, $-\infty < t < \infty$) such that d′ (z) with t^{max} is a concave curve assuming virtually no effect in the optimization process. Realistic values of t lies between -10 and 10. For $t < 0$ the function is convex, for $t = 0$ the function is linear and for $t > 0$ the function is concave. R^2 is the coefficient of determination and z is a standardized parameter representing the distance of the estimated response from its target in units of the maximum allowable deviation. This parameter depends on the response type and is defined as:

$$z_i(x) = \begin{cases} \frac{\hat{y}_i(x) - y_i^{min}}{y_i^{max} - y_i^{min}}, & (for\ STB) \\ \frac{y_i^{max} - \hat{y}_i(x)}{y_i^{max} - y_i^{min}}, & (for\ LTB) \end{cases} \qquad with\ y_i^{min} \leq \hat{y}_i(x) \leq y_i^{max} \quad (8)$$

where y_i^{max} and y_i^{min} represent the maximum and minimum values of the estimated response ($\hat{y}_i$(x)), respectively. Eq. (8) between 0 and 1.

In the present study, in order to consider the predictive ability of each response model, R^2 was substituted by the coefficient of determination in prediction (Q^2_{LOO}). t^{max} was fixed equal to 10. The values of *t* for each model were chosen considering the importance of the response.

In this approach, the overall minimal level of satisfaction is reached following the formulation:

$$\max_{x \in \Omega}(\min\,[d_1\,\{(\hat{y}_1(x)\}, d_2\{(\hat{y}_2(x)\}, \ldots d_n\{(\hat{y}_n(x)\}]) \quad (9)$$

where x represents the combination of experimental conditions within the experimental domain Ω.

In the present study, only LTB and STB response types were considered for both approaches. The minimum and maximum values for each responses (y_i^{max} and y_i^{min}) were set at the extreme values of each estimated response.

The linear regression models, ANOVA, response surfaces and desirability functions were calculated by Modde 6.0 (Umetrics, Umea, Sweden), and MATLAB R2013 (The MathWorks Inc., Natick, USA).

3 RESULTS AND DISCUSSION

3.1 Regression models

The results of the experiments are summarized in Table 2. As a response for the model, the value of η* was uniquely taken at the frequency of 200 rad/s, since the analysis was more stable at this frequency.

For each experimental response, a reduced subset model was obtained considering the only terms that resulted significant. Table 3 shows regression coefficients for each experimental response related to the scaled and centered variables.

In order to achieve the best subset model, some terms were included even if they did not result significant to preserve the principal of hierarchy. A model is considered hierarchical if the presence of significant higher-interactions or higher-order terms requires the inclusion of the lower-order terms within the higher-order ones.

All the obtained reduced regression models were statistically significant at 95% level, without showing any lack of fit at the same probability [12,21]. The residual distributions, as shown in Figure 2, did not reveal evident anomalies. The normal distribution for the residuals was confirmed by the Shapiro-Wilk normality test at 99 % confidence level [39].

Q^2_{LOO} was used to select the best subset model for each response. Therefore, this statistic resulted in the highest prediction power for each model (Table 4). Moreover, each model showed relatively high R^2 and R^2 adjusted (R^2 adj), offering an acceptable explanation of the total variance.

Table 2 Results of the central composite design.

Experiment	US (µm)	SS (rpm)	FR (g/min)	T (℃)	η* (kPa.s)	CD (mmol/cm^3)	GF (wt %)	M100 (MPa)	TS (MPa)	Eb (elongation %)
Experiments based on a full factorial design at two levels										
E1	5	150	4	130	3.26	0.043	83.0	3.22	4.52	132
E2	12	150	4	130	1.90	0.028	75.5	2.71	5.37	169
E3	5	250	4	130	3.53	0.040	85.0	3.43	4.21	117
E4	12	250	4	130	1.34	0.020	74.0	2.53	5.88	179
E5	5	150	8	130	4.03	0.043	84.2	3.49	4.43	127
E6	12	150	8	130	2.23	0.032	77.0	3.01	4.71	136
E7	5	250	8	130	3.79	0.031	83.2	3.50	3.86	112
E8	12	250	8	130	1.63	0.024	76.5	2.56	6.52	196
E9	5	150	4	210	3.09	0.027	81.3	3.19	4.02	124
E10	12	150	4	210	1.70	0.028	76.1	2.48	4.70	161
E11	5	250	4	210	1.75	0.028	79.1	3.12	6.10	159
E12	12	250	4	210	1.00	0.018	74.4	2.86	6.13	179
E13	5	150	8	210	3.35	0.035	83.6	3.19	3.52	112
E14	12	150	8	210	2.07	0.027	77.7	2.62	4.89	162
E15	5	250	8	210	2.01	0.023	77.8	2.89	6.06	170
E16	12	250	8	210	1.28	0.020	74.8	2.60	6.22	189
Axial experiments (distance ± 1 from the center)										
E17	5	200	6	170	3.77	0.037	84.1	3.38	4.11	116
E18	12	200	6	170	2.16	0.026	77.4	3.05	5.65	160
E19	8.5	150	6	170	3.01	0.033	80.7	3.10	4.27	133
E20	8.5	250	6	170	1.81	0.023	77.4	3.03	6.02	163
E21	8.5	200	4	170	2.09	0.029	77.7	2.83	5.92	174
E22	8.5	200	8	170	2.54	0.030	79.3	2.90	4.96	152
E23	8.5	200	6	130	2.62	0.038	80.5	3.20	4.97	150
E24	8.5	200	6	210	1.58	0.027	77.8	2.87	6.35	178
Central experiments										
C1	8.5	200	6	170	2.37	0.033	79.1	2.97	5.42	160
C2	8.5	200	6	170	2.59	0.028	78.6	2.84	5.09	158
C3	8.5	200	6	170	2.48	0.027	78.6	3.13	5.39	142
C4	8.5	200	6	170	2.51	0.027	77.9	3.19	5.00	140

Table 3 Regression coefficients and standard error (SE) for each experimental response related to the scaled and centered variables.

Experimental response	η*	SE	CD	SE	GF	SE	M100	SE	TS	SE	Eb	SE
Constant	2.45	0.05	0.0295	0.0004	79.0	0.2	3.05	0.03	5.3	0.1	153	3
US	-0.74	0.04	-0.0047	0.0005	-3.2	0.2	-0.28	0.02	0.51	0.09	20	2
SS	-0.36	0.04	-0.0038	0.0005	-0.9	0.2	-0.03	0.02	0.59	0.09	12	2
FR	0.18	0.04	0.0002	0.0005	0.4	0.2	0.02	0.02	_	_	-2	2
T	-0.36	0.04	-0.0037	0.0005	-0.9	0.2	-0.10	0.02	0.20	0.09	6	2
US*US	0.40	0.09	_	_	1.1	0.4	0.13	0.05	-0.3	0.1	-14	5
SS*SS	_†	_	_	_	_	_	_	_	_	_	_	_
FR*FR	_	_	_	_	-1.1	0.4	-0.22	0.05	_	_	_	_
T*T	-0.47	0.09	_	_	_	_	_	_	_	_	12	5
US*SS	-0.02E-05	0.04	-0.0004	0.0005	0.2E-01	0.2	-0.01	0.02	0.08	0.09	3	2
US*FR	_	_	0.0009	0.0005	0.3	0.2	_	_	_	_	_	_
US*T	0.21	0.04	0.0021	0.0005	0.8	0.2	0.06	0.02	-0.20	0.09	-4	2
SS*FR	_	_	-0.0012	0.0005	-0.4	0.2	-0.07	0.02	_	_	5	2
SS*T	-0.19	0.04	_	_	-0.7	0.2	0.03	0.02	0.37	0.09	6	2
FR*T	_	_	0.0003	0.0005	_	_	-0.06	0.02	_	_	_	_
US*SS*FR	_	_	0.0016	0.0005	0.4	0.2	_	_	_	_	_	_
US*SS*T	0.15	0.04	_	_	0.4	0.2	0.10	0.02	-0.32	0.09	-9	2
US*FR*T	_	_	-0.0012	0.0005	_	_	_	_	_	_	_	_
SS*FR*T	_	_	_	_	_	_	_	_	_	_	_	_

† The character '_' represents the coefficient removed from the reduced model.

Table 4 Coefficients of determinations of reduced models

Response	R^2	R^2 adj	Q^2_{LOO}	$y_i^{min\dagger}$	$y_i^{max\dagger}$	Optimal
η*	0.98	0.96	0.94	0.80	4.16	Min
CD	0.93	0.89	0.86	0.018	0.044	Min
GF	0.98	0.95	0.88	73.8	85.3	Min
M100	0.94	0.90	0.88	2.52	3.67	Max
TS	0.87	0.81	0.74	3.69	6.46	Max
EB	0.91	0.85	0.72	194	102	Max

† The value of y_i^{min} and y_i^{max} were computed for each response

3.1.2 D-GTR

η* was determined as a function of the angular frequency and followed the power law behavior. Therefore, the experimental data were fitted according to the following equation:

$$\eta^* = K\omega^{n-1} \quad (10)$$

where *ω* represents the frequency and *K* and n are empirical constants (n < 1).

The constant *K* in Eq. 10, representing a measure of flow resistance, could have been used as an additional experimental response for the model. This parameter allowed us to consider the behavior of the rubber in the entire region of the studied frequencies. Figure 3 shows the dependence of η* on the frequency ω and the power law fit for three samples chosen as representative ones.

Nevertheless, this additional response (K) showed an analogous behavior as η* at 200 rad/s with the same significant terms for the fitted reduced model. For this reason, it was decided to uniquely consider η* during the optimization process.

The analysis of the η*, GF and CD were performed directly on the material after the devulcanization, since these values give information on the rupture of the crosslink network. The η*, as function of angular frequency, is a measure of the resistance to flow. In particular η* decreases with a decrease of molecular weight, crosslink density and gel fraction. The GF represents the insoluble fraction after removing the sol fraction. It decreases with the increase of network breakage and with the increase of polymeric soluble fraction. Similarly, the CD represents the effective number of chains per unit of volume and it decreases with the increase of devulcanization.

From the reduced models (Table 3), it can be seen that all process variables have influence on the devulcanization process. The ultrasonic amplitude showed the highest effect, acting with a negative trend on D-GTR properties. Indeed, as already observed in [4], the ultrasonic devulcanization increases with the ultrasonic amplitude. The effects of screw speed and temperature were found to be less important despite the fact that these process variables acted in the same direction as the ultrasonic amplitude. Indeed these two process variables are responsible for thermal and mechanical degradation and decrosslinking [8,9]. The effect of flow rate was observed to be less important and acting in opposite direction, since the flow rate increase decreases the residence time of the material within the extruder, decreasing the devulcanization treatment time.

In order to investigate in more detail the relative effect of degradation of the main chain and of the crosslink network, the normalized gel fraction versus the normalized crosslink density (Figure 4) was studied. Since it is difficult to determine the type of bond rupture during the ultrasonic treatment of GTR, the dependence of experimental normalized gel fraction versus normalized crosslink density was analyzed and compared to the Horikx function, that was derived from the statistical theory dealing with the gel fraction–crosslink density relationship [34,40-45]. In our case, it was possible to calculate only the function for the main chain brakeage, but not the one for the selective crosslink breakage, since the value of M_n is not available for the GTR that represents a waste and vulcanized material. Thus, in Figure 4, the line indicates the Horikx function based on the main chain breakage only. Experimental data are indicated by symbols. It is seen that experimental results lie above the Horikx function [44]. Therefore, it can be concluded that the ultrasonic treatment preferentially cleaved the crosslink network with some breakage of the main chain. However, it is impossible from this plot to define types of crosslink breakage (mono-sulfidic, di-sulfidic and poly-sulfidic). In addition, it was difficult to experimentally measure the amount of different type crosslink breakage on D-GTR. In that regard, a previous study [45] (conducted on a model SBR rubber) indicated that the ultrasonic devulcanization causes a significant decrease of poly-sulfidic and mono-sulfidic crosslinks indicating that ultrasonic devulcanization takes place indeed.

3.1.3 R-GTR

The analysis of M100, TS and Eb were performed on the material R-GTR after compounding and revulcanization. Generally, the compound recipe and crosslink network type are the main parameters influencing all these mechanical properties [46]. However, in our case, the filler content and recipe of the R-GTR were kept constant. Therefore, the mechanical properties were strictly correlated to the devulcanization effect induced by the ultrasonic treatment.

M100 is a measure of the tensile properties at 100 % of elongation. TS and Eb represent the final mechanical properties. They define the failure point of the vulcanizates.

As seen from Table 3, M100 follows a reduced model that is similar to the one observed for all the responses evaluated on the D-GTR. The increase of the ultrasonic amplitude, screw speed and temperature and the decrease of the flow rate led to lower values of M100. Several researches have already observed that the modulus increases with the crosslink density and gel fraction of the material. Furthermore, the crosslink density and gel fraction of revulcanizates are highly correlated with the correspondent devulcanizates, as long as the curing recipe is kept constant [5,47]. Therefore, also in this case higher values of gel fraction and crosslink density of D-GTR led to higher values of R-GTR. Although M100 of R-GTR resulted to be correlated with the crosslink density and gel fraction of the D-GTR, it is clear that TS and Eb behaved differently. Indeed, the main significant process variables had completely opposite influence on these two properties. These final mechanical properties were strongly influenced by the degree of devulcanization. More breakage of the three-dimensional network can generate more active sites that can be cured during the revulcanization process, increasing the compatibility among the D-GTR particles.

In order to better understand the trend of the response surfaces, 3D plot are shown in Figure 5. In these surfaces each response was plotted as function of US and T, fixing the values of FR at center level (0) and SS at the highest one (+ 1).

In Figure 5 it is clear that the mechanical properties are strongly dependent on the structure properties. Namely, the CD, GF and η* showed similar behaviors, since their decrease was observed with an increase of T and US. On the other hand, the mechanical properties did not show a unique behavior. The M100 showed significant decrease at high T and US, while the opposite was observed for TS and Eb. As already observed in the previous study [5] this different behavior of the mechanical properties of the R-GTR can be explained by considering their correlation with the structure of the D-GTR. The reduction of CD and GF is generally associated to an increase of the sol fraction. This soluble polymeric fraction, along with the gel of lower crosslink density, provides enough active sites that can be re-cured, increasing the compatibility among various D-GTR particles, resulting in better final properties. On the other hand, the M100 behaves in opposite manner since this property shows higher values at higher values of CD and GF.

3.2 Validation

A validation was carried out in order to test the reduced models predictive power within the studied domain. In addition, some experiments were carried out to evaluate the applicability of the model outside the studied domain.

The conditions used for validation experiments are reported in Table 5. These experiments were fixed by selecting combinations of independent variables within the experimental domain. Moreover, the predictive power of the models was tested outside the experimental region, removing the most influential process variable. Therefore, two experiments (v1 and v2) were carried out without applying any ultrasonic treatment.

The results of these validation experiments are shown in Figure 6. In particular, the experimental results of the validation experiments (v1-v7) are represented by symbols and are compared to the range of values predicted by each model, here presented as bars. It can be seen that the validation experiments carried out within the experimental domain (v3-v7) were in good agreement with the range of predicted values. Moreover, some models showed an acceptable predictive capacity outside the experimental range (v1 and v2).

Table 5 Validation experiment conditions.

Experiment	Ultrasonic Amplitude (µm)	Screw Speed (rpm)	Flow rate (g/min)	Temperature (℃)
Experiments out of the experimental domain				
v1	0	250	8	130
v2	0	200	8	170
Experiments within the experimental domain				
v3	8.5	250	6	170
v4	8.5	200	6	170
v5	12	250	6	130
v6	12	200	6	170
v7	12	150	8	130

3.3 Optimization

In the previous sections, our attention was focused on modeling each response as a function of the input process variables. Two different behaviors were generally observed, as seen in Figure 5. Moreover, in Figure 7 it can be observed that the optimal condition as a function of US and T is different for each response.

Although, for practical applications, the process variables could be varied in order to achieve the optimal conditions for a desired property, in the present study a multiple response optimization approach was attempted. In particular, this optimization was carried out considering a possible application of the D-GTR in new tires. Therefore, it was decided to assign more importance to the M100 and TS. The weights and parameters used for the two different desirability function approaches are shown in Table 6. The results of the optimization are listed in Table 7.

Although the two desirability function approaches gave different overall degree of satisfaction, the two approaches gave comparable results in term of optimal process conditions. In order to maximize the value of M100 and TS, it is necessary to keep a relatively low value of US, sufficient to reduce the network density and to increase the number of active sites so D-GTR can be revulcanized, without introducing an excessive degradation.

Table 6 Parameters for desirability functions

Response	Type of desirability function	$y_i^{min\dagger}$	$y_i^{max\dagger}$	w‡	t§
η*	STB	0.80	4.16	1	-1
CD	STB	0.018	0.044	1	-1
GF	STB	73.8	85.3	1	-1
M100	LTB	2.52	3.67	3	-3
TS	LTB	3.69	6.46	3	-3
EB	LTB	194	102	1	-1

† The value of y_i^{min} and y_i^{max} were computed for each response, using the reduced subset models reported in the Results and Discussion section.
‡ Weights for the Derringer and Suich approach
§ Value of t parameter for the Kim and Lin approach

Table 7 Desirability functions optimization results

Parameter	Derringer and Suich	Kim and Lin
Optimal Conditions (US, SS, FR, T)	(7.2, 250, 5.5, 210)	(5, 250, 5.6, 202)
Predicted responses (η*, CD, GF, M100, TS, Eb)	(1.22, 0.023, 77.4, 3.03, 6.39, 183)	(2.16, 0.027, 80.2, 3.27, 5.87, 155)
Desirability function value optimal conditions d (η*, CD, GF, M100, TS, Eb)	(0.87, 0.79, 0.69, 0.09, 0.93, 0.88) †	(0.55, 0.73, 0.48, 0.48, 0.82, 0.80) †
Overall degree of satisfaction	0.71	0.48

† Each d (η*, CD, GF, M100, TS, Eb) was already weighed considering the parameters in Table 6.

4 CONCLUSIONS

The aim of the present study was to investigate a green and continuous ultrasonic devulcanization process that could be carried out in a short time adjusting the process variables in order to optimize specific required conditions. Ultrasonic-assisted devulcanization in a twin-screw extruder was studied and modeled using a face-centered central composite design and desirability functions. Several responses on the D-GTR and on R-GTR were chosen as responses and reduced regression models were obtained by regression analysis. The properties of the D-GTR and R-GTR were influenced by all the process variables as well as interaction effects between them. However, the US was found to be the most influencing process variable for the described screw configuration. Different behaviors were observed for the various responses. For this reason, an optimization was performed in order to maximize the TS and M100, considered the most important parameters for reuse of D-GTR. A relatively low value of US was required to reduce the network density without introducing an excessive degradation of the tire rubber.

This study has an important outcome since the approach presented here can be applied to the devulcanization of any type of GTR in order to reach the optimal desirable properties for different applications.

ACKNOWLEDGEMENTS

The authors are grateful to the financial support provided by the National Science Foundation (NSF) under Grant CMMI-1131342 and to Akrochem Corporation for providing compounding ingredients. The authors also thank Dr. Paola Caracino for the support given to our research.

REFERENCES

1. B. Adhikari, D. De, S. Maiti, Reclamation and recycling of waste rubber, Prog. Polym. Sci. 25 (2000) 909-948.
2. V. Rajan, W.K. Dierkes, R. Joseph, J.W.M. Noordermeer, Science and technology of rubber reclamation with special attention to NR-based waste latex products, Prog. Polym. Sci. 31 (2006) 811-834.
3. A.K. Naskar, S.K. De, A.K. Bhowmick, P.K. Pramanik, R. Mukhopadhyay, Characterization of ground rubber tire and its effect on natural rubber compound, Rubber Chem. Technol.73 (2000) 902-911.
4. A.I. Isayev, Recycling of Rubbers, in: J.E. Mark, B. Erman, M. Roland (Eds.), The Science and Technology of Rubber, fourth ed., Elsevier Academic Press, Boston: 2014., pp. 697-764.
5. A.I. Isayev, T. Liang, T.M. Lewis, Effect of particle size on ultrasonic devulcanization in twin-screw extruder, Rubber Chem. Technol. 87 (2014) 86-102.
6. K. Formela, M. Cysewska, J. Haponiuk, A. Stasiek, The influence of feed rate and shear forces on the devulcanization process of ground tire rubber (GTR), Polimery 58 (2013)906-912.
7. K. Formela, M. Cysewska, J. Haponiuk, The influence of screw configuration and screw speed of co-rotating twin screw extruder on the properties of products obtained by thermomechanical reclaiming of ground tire rubber, Polimery 59 (2014) 170-177.
8. J. Shi, K. Jiang, D. Ren, H. Zou, Y. Wang, X. Lv, L. Zhang, Structure and performance of reclaimed rubber obtained by different methods, J. Appl. Polym. Sci. 129 (2013) 999-1007.

9. G. Tao, Q. He, Y. Xia, G. Jia, H. Yang, W. Ma, The effect of devulcanization level on mechanical properties of reclaimed rubber by thermal-mechanical shearing devulcanization, J. Appl. Polym. Sci. 129 (2013) 2598-2605.

10. B. Maridass, Cure modeling and mechanical properties of counter rotating twin screw extruder devulcanized ground rubber tire-natural rubber blends, J. Polym. Res. 16 (2009) 133-141.

11. H. Si, T. Chen, Zhang Y, Effects of High Shear Stress on the Devulcanization of Ground Tire Rubber in a Twin-Screw Extruder, J. Appl. Polym. Sci. 128 (2013) 2307-2318.

12. G.P.E. Box, W.G. Hunter, J.S. Hunter, Statistics for Experimenters, second ed., Wiley, Hoboken, New Jersey: 1978.

13. B. Maridass, B.R. Gupta, Effect of extruder parameters on mechanical properties of revulcanized ground rubber tire powder. Polimery 52 (2007) 456-460.

14. B. Maridass, B.R. Gupta, Process optimization of devulcanization of waste rubber powder from syringe stoppers by twin screw extruder using response surface methodology, Polym. Compos 29 (2008) 1350-1357.

15. H. Yazdani, I. Ghasemi, M. Karrabi, H. Azizi, G.R. Bakhshandeh, Continuous devulcanization of waste tires by using a co-rotating twin screw extruder: Effects of screw configuration, temperature profile, and devulcanization agent concentration, J. Vinyl. Addit. Technol. 19 (2013) 65-72.

16. B. Maridass, B.R. Gupta, Performance optimization of a counter rotating twin screw extruder for recycling natural rubber vulcanizates using response surface methodology, Polym. Test. 23 (2004) 377-385.

17. A.I. Isayev, S.P. Yushanov, J. Chen, Ultrasonic devulcanization of rubber vulcanizates. I. Process model. J. Appl. Polym. Sci. 59 (1996) 803-813.

18. A.I. Isayev, S.P. Yushanov, J. Chen, Ultrasonic devulcanization of rubber vulcanizates. II. Simulation and experiment, J. Appl. Polym. Sci. 59 (1996) 815-824.

19. S.P. Yushanov, A.I. Isayev, S.H. Kim, Ultrasonic Devulcanization of SBR Rubber: Experimentation and Modeling Based on Cavitation and Percolation Theories, Rubber. Chem. Technol. 71 (1998) 168-190.

20. I. Khuri, J.A. Cornell, Response Surfaces: Designs and Analyses, second ed., Marcel and Dekker Inc., New York, 1996.

21. R.H. Myers, D.C. Montgomery, Response surface methodology: process and product optimization using designed experiments, second ed. Wiley, New York, 2002.

22. P.J. Brandvik, Statistical simulation as an effective tool to evaluate and illustrate the advantage of experimental designs and response surface methods, Intell. Lab. Syst.42 (1998) 51–61.

23. Leardi R. Experimental design in chemistry: A tutorial, Anal. Chim. Acta 652 (2009) 161–172.

24. I. Mangili, E. Collina, M. Anzano, D. Pitea, M. Lasagni, Characterization and supercritical CO2 devulcanization of cryo-ground tire rubber: Influence of devulcanization process on reclaimed material, Polym. Degrad. Stabil.102 (2014) 15-24.

25. I. Mangili, M. Oliveri, M. Anzano, E. Collina, D. Pitea, M. Lasagni, Full factorial experimental design to study the devulcanization of ground tire rubber in supercritical carbon dioxide, J. Supercrit. Fluids 92 (2014) 249-256.

26. N.R Draper, Center points in second-order response surface designs, Technometrics 24 (1982) 127-133.

27. J.A. Dec, N.M. Thornblom Autonomous Aerobraking: Thermal Analysis and Response Surface Development. Adv. Astronaut Sci.142 (2012) 483-498.

28. L.A. Dillon, V.N. Stone, L.A. Croasdell, P.R. Fielden, N.J. Goddard, C.L. Thomas, Optimisation of secondary electrospray ionisation (SESI) for the trace determination of gas-phase volatile organic compounds, Analyst 135 (2010) 306-314.

29. E. Cagigal, L. González, R.M. Alonso, R.M. Jiménez, Experimental design methodologies to optimise the spectrofluorimetric determination of Losartan and Valsartan in human urine, Talanta 54 (2001) 1121-1133.

30. L. Eriksson, E. Johansson, N. Kettaneh-Wold, C. Wikström and S. Wold, Design of Experiments Principles and Applications, third ed., Umetrics Academy, Umea, 2008.

31. I.E. Frank, R. Todeschini, The data analysis handbook, Elsevier, Amsterdam, 1994.

32. I. Batmaz, S. Tunali, Second-Order Experimental Designs for Simulation Metamodeling, Simulation:78 (2002) 699-715.

33. J.L. Valentín, J. Carretero-González, I. Mora-Barrantes, W. Chassé, K. Saalwa□chter, Uncertainties in the determination of crosslink density by equilibrium swelling experiments in Natural Rubber. Macromolecules 41 (2008) 4717-4729.

34. E. Bilgili, H. Arastoopour, B. Bernstein, Pulverization of rubber granulates using the solid state shear extrusion process. Part II. Powder characterization. Powder Technol. 115 (2001) 277-289.

35. G. Kraus, Swelling of filler-reinforced vulcanizates, J. Appl. Polym. Sci.7 (1963) 861-871.

36. N.R. Costa, J. Lourenço, Pereira. Desirability function approach: A review and performance evaluation in adverse conditions, Chemometr. Intell. Lab. 107 (2011) 234-244.

37. G. Derringer, R. Suich, Simultaneous Optimization of Several Response Variables. J. Qual. Technol.12 (1980) 214-219.

38. K.J. Kim, D. Lin, Simultaneous optimization of multiple responses by maximining exponential desirability functions, J. Roy. Stat. Soc. C-App.49 (2000) 311-325.

39. S.S. Shapiro, M.B. Wilk, An analysis of variance test for normality (complete samples). Biometrika 52 (1965) 591-611.

40. X. Sun, A.I. Isayev, Ultrasound devulcanization: comparison of synthetic isoprene and natural rubbers, J. Mater. Sci.42 (2007) 7520-7529.

41. S. Ghose, A.I. Isayev, Ultrasonic devulcanization of carbon black filled polyurethane rubber, J. Elastom. Plast.36 (2004) 213-239.

42. VV. Yashin, A.I. Isayev, A model for rubber degradation under ultrasonic treatment: part II. Rupture of rubber network and comparison with experiments, Rubber Chem. Technol.73 (2000) 325-338.

43. A.I. Isayev, S. P. Yushanov, S.H. Kim, V.L. Levin, Ultrasonic devulcanization of waste rubbers: experimentation and modeling, Rheol. Acta 35 (1996) 616-630.

44. M.M. Horikx, Chain scissions in a polymer network, J. Polym. Sci. 19 (1956) 445-454

45. V. Yu Levin, S. H. Kim, A. I. Isayev, Effect of Crosslink Type on the Ultrasound Devulcanization of SBR Vulcanizates. Rubber Chem. Techol. 70 (1997) 641-649.

46. A.Y. Coran, Vulcanization, in: J.E. Mark, B. Erman, M. (Eds.), The Science and Technology of Rubber, fourth ed. Elsevier Academic Press,Boston: 2014., pp. 337-381.

47. W. Feng, A.I Isayev, In-situ ultrasonic compatibilization of unvulcanized and dynamically vulcanized PP/EPDM blends, Polym. Eng. Sci. 46 (2006) 8-16.